V. Muscarello, G. Quaranta
Wing-Pilot Vertical Bounce in Tiltrotors
Journal of Guidance Control and Dynamics, Vol. 41, N. 8, 2018, p. 1731-1743
doi:10.2514/1.G002960

Wing–Pilot Vertical Bounce in Tiltrotors

Vincenzo Muscarello*, Giuseppe Quaranta†

Politecnico di Milano, 20156 Milano, Italy

The basic mechanism of the vertical bounce in tiltrotors in hovering flight is discussed. This rotorcraft-pilot coupling phenomenon arises when the pilot's biomechanics interact with the airframe elastic modes, in particular with the first symmetric wing bending mode. For this reason it can be referred to as wing-pilot vertical bounce. This work proposes a simple mathematical model to predict the phenomenon. The XV-15 tiltrotor is used as benchmark. The closed-loop pilot-vehicle system shows that the direct effect of a change in collective input, through a vertical power-lever, results in a nearly immediate change in thrust, which accelerates the aircraft exciting the symmetric wing bending mode and, in turn, the pilot biomechanics, leading to a feedback path that could easily become unstable. Robust stability analyses are performed to take into account the large variability of some influential parameters. The tiltrotor shows a significant proneness to this rotorcraft-pilot coupling problem which must be considered from the earliest phases of the design especially when fly-by-wire architectures are considered. Means of prevention, considering both active and passive devices, are investigated and compared.

Nomenclature

a_z^{seat}	vertical acceleration measured at the pilot's seat, ft $\cdot$ s^{-2}
$\mathbf{C_1}, \mathbf{C_2}$	damping matrices of the tiltrotor model
C	viscous coefficient of hydraulic damper on the power-lever, lbf $\cdot$ in $\cdot$ sec $\cdot$ rad^{-1}

*PostDoc, Dipartimento di Scienze e Tecnologie Aerospaziali.

†Associate Professor, Dipartimento di Scienze e Tecnologie Aerospaziali.

c_w	tiltrotor wing chord, ft
DL	download force acting on the wing, lbf
EI_{xx}	out-of-plane wing bending stiffness, lb $\cdot$ in^2
$\mathbf{f_1}, \mathbf{f_2}$	input forces of the tiltrotor model
G_0	gear ratio between power-lever vertical tip displacement and collective pitch rotation, deg $\cdot$ in^{-1}
H_{LTF}	seat vertical acceleration loop transfer function
H_{NF}	transfer function of the notch filter
$H_{\ddot{z}\vartheta_0}$	transfer function of the tiltrotor between collective pitch and seat vertical acceleration, ft $\cdot$ s^{-2} $\cdot$ rad^{-1}
I_b	flapping inertia per blade, slug $\cdot$ ft^2
J_{xx}	inertia lumped on the wing tip about global x axis, slug $\cdot$ ft^2
$\mathbf{K}$	stiffness matrix of the tiltrotor model
l	semi-span wing length, ft
l_M	rotor mast length, ft
$\mathbf{M}$	mass matrix of the tiltrotor model
M_1	mass lumped on the wing root, lb
M_2	mass lumped on the wing tip, lb
N_b	number of blades per rotor
$\mathbf{p}$	vector of trim parameters
Q	notch filter quality factor
R	rotor radius, ft
$\mathbf{u}$	state vector of the tiltrotor model
v	rotor induced velocity, ft $\cdot$ s^{-1}
w	vertical elastic deflection of the wing, ft
z	vertical displacement at the wing root, ft
β_n	nacelle angle, deg
δ_{PL}	power-lever deflection, in
ξ_p	pilot biomechanical damping ratio
λ_u	axial inflow perturbation

γ	Lock number
ϑ_0	collective pitch, rad
Ω	rotor speed, rpm
ω_h	cut-off frequency between voluntary–involuntary pilot model, rad $\cdot$ sec^{-1}
ω_p	pilot biomechanical frequency, rad $\cdot$ sec^{-1}
ω_{NF}	notch filter frequency, rad $\cdot$ sec^{-1}
τ_p	pilot biomechanical time constant, sec
μ	slope in gain at the notch frequency
μ_∞	notch filter non dimensional gain value for infinite frequency

I. Introduction

Several pilot-in-the-loop aeroelastic coupling mechanisms have been encountered during the development of tiltrotor aircraft, from the early design and testing of the XV-15 technology demonstrator [1] to the V-22 experimental flight tests [2]. On the BA609 (now AW609), the design methodology has benefited from the past experience, and pilot-in-the-loop stability analyses have been considered from the early design stage [3], to ensure that Rotorcraft Pilot Coupling (RPC) problems did not degrade the overall stability of the vehicle.

In tiltrotors, as well as in helicopters, the pilot might introduce inadvertent or unintentional control inputs caused by vibrations in the cockpit. These phenomena are called Pilot-Assisted Oscillations (PAOs). The involved vibrations typically occur at frequencies above those of the human operator bandwidth, between 2 and 8 Hz according to Ref. [4]. PAOs phenomena differ from the most widely known Pilot-Induced Oscillations (PIOs), in which the oscillatory behavior of the vehicle results from commands intentionally introduced by the pilot as a result of misinterpreted or contradictory vehicle response cues. While PIO mechanisms are analyzed by means of rigid body vehicle models affecting the flight mechanics modes, PAO phenomena require aeroelastic models in order to represent the higher structural mode frequencies.

Both PIO and PAO phenomena fall under the definition of Aircraft-Pilot Couplings (APCs) or Rotorcraft-Pilot Couplings (RPCs) when specifically referred to rotary wing aircraft. PIO and PAO have been widely

investigated in relation with fixed-wing aircraft. In recent times, rotary-wing aircraft PIOs have received considerable attention. Research on PAO phenomena for rotorcraft is ongoing. In 2007, Walden [5] presented an extensive discussion of aeromechanical instabilities that occurred on several rotorcraft during their development and acceptance by the US Navy, including the CH-46, UH-60, SH-60, CH-53, V-22, and AH-1. A database of PIO and PAO incidents that have occurred to fixed-and rotary-wing aircraft is reported in [6]. Most of those events occurred in the PAO frequency band and involved the involuntary participation of the pilot, often interacting with the Flight Control System (FCS). In many examples, any attempt to reduce the vehicle's PAO tendency was conducted on a case-by-case basis, and it was sometimes addressed by procedural mitigation. However, several important structural interventions on the design of aircraft to solve PAO problems were also developed as an outcome of flight test campaigns [2, 5].

In this paper, a known PAO phenomenon peculiar to helicopters is now investigated for tiltrotors during hovering flight: the *vertical bounce*. It is caused by a pulsating thrust induced by an oscillation of collective control lever introduced by the pilot. Several studies have been performed on RPC both through numerical analysis [7] and experimental test [8]. The key implication of RPC on helicopters has been identified as the reduction of the phase margin of the main rotor coning mode in the collective pitch-heave loop transfer function (see Ref. [9]). Muscarello et al. [9] also showed that the reduction of stability margins is rooted in the coupling of the first collective flap (or coning) mode of the main rotor and the biodynamic mode of the pilot's arm holding the collective control inceptor. Helicopters specifically prone to vertical bounce phenomena are those with a coning frequency close to the pilot's biomechanical pole at about 2.5–4 Hz; i.e. medium/heavy lift helicopters with large main rotor radii and low rotation speeds. Recently, a vertical bounce phenomenon was experienced by a Danish AW101 helicopter during landing in degraded visual environment[a]. Although the crew was not seriously injured, the helicopter was destroyed. The accident report confirmed that the vertical bounce occurred at 3.65 Hz.

On classical stiff-in-plane gimballed rotors the coning mode frequency is over the pilot's voluntary/involuntary bandwidth, but the vertical bounce phenomenon may still arise if the pilot's biomechanics interact with the airframe elastic modes, in particular with the first Symmetric Wing Bending (SWB) mode. In Ref. [3]

[a]See the website http://ing.dk/artikel/rystelser-i-forsvarets-ulykkeshelikopter-gjorde-pilot-til-ufrivillig-plejlstang-177495 (in Danish).

Parham et al. list the frequencies, obtained through a detailed NASTRAN model of the AW609 airframe in airplane and helicopter modes (AP/HE-MODE). The first SWB frequency ranges from 3.35 Hz in APMODE to 3.02 Hz in HEMODE. Similar results are found for the XV-15 [10, 11]. Consequently, the vertical bounce may appear as an interaction between the airframe first SWB mode and the pilot's unintentional control input on the collective lever produced by the cockpit vertical accelerations.

Flight test of the V-22 revealed several mechanisms for pilot biomechanical coupling with the airframe dynamics [2], involving a 1.4 Hz lateral oscillation on the ground, a 3.4 Hz lateral oscillation in APMODE and a 4.2 Hz longitudinal oscillation in APMODE. No PAO phenomenon on the vertical axis has been noticed. However, it must be highlighted that in the V-22 Osprey the rotor collective pitch is controlled through a Thrust Command Lever (TCL) as done for conventional fixed wing aircraft, i.e. a lever that is activated through fore/aft displacement. Conversely, on the AW609 civil tiltrotor (as on the XV-15) there is a vertical Power Lever (PL) that acts as a collective pitch lever in helicopter mode and as thrust control in airplane mode, and that is activated through an essentially vertical displacement. The vertical movement of the PL increases the possibility of triggering a PAO phenomenon on the vertical axis, since it creates a connection between the vertical acceleration at the pilots' seat and the rotor collective through the vertical response of the pilots' upper limbs [12]. As far as the authors know, during flight tests the XV-15 did not have any accidents rooted to pilot biomechanical coupling, even though some were expected [2]. This absence may be related to the high equivalent damping caused by friction in the complex set of mechanical linkages that composed the control chain [3]. However, significant biomecahnical problems may arise when switching to fly-by-wire architectures, as for the V-22 and AW609 [2, 3, 5].

This work shows how it is possible to analyze the vertical bounce phenomenon in tiltrotors through a simple closed-loop system representing the main dynamics on the vertical axis. Exploiting the large availability of data on XV-15, it was possible to build a detailed aeroservoelastic model of this tiltrotor that confirms that the simple analytical model well represents the low-frequency dynamics. Owing to its simplicity, the model can be exploited in the earliest stages of the design, when only the main parameters of the aircraft are known. This will help to prevent vertical bounce before reaching the flight test phase. The last section brings the paper to closure by suggesting means of prevention to avoid the vertical bounce instability. Two solutions are proposed, based on the implementation of a structural notch filter at the FCS

level or by adding a hydraulic damper to the PL. It is useful to note, that the effect of friction can be often linearized as an equivalent damping, leading to an effect similar to that of a hydraulic damper. Pros and cons, of the two analyzed solutions, are discussed.

II. Modeling pilot-in-the-loop aeroelastic phenomena

Pilot-in-the-loop phenomena can be investigated through the pilot-control device dynamics in the feedback loop with the aircraft model. The Pilot-Vehicle System (PVS) can be represented in a simple block diagram, as shown in Fig. 1. The pilot is generally split in two parts since the control devices are actuated as a consequence of two logically distinct contributions. The first contribution is the result of the intentional action performed by the pilot to control the vehicle based on the perceived cues to perform the desired task. The second contribution originates from cockpit oscillations produced by the aircraft and filtered by the pilot's biodynamics. The arms of the pilot oscillate while holding the control devices, generating involuntary controls. Voluntary and involuntary inputs are introduced in the aircraft dynamics by means of the contact forces ($\boldsymbol{F_C}$) exerted by the pilot on the cockpit inceptors. The resulting control inceptor deflections are the pilot's demand ($\boldsymbol{\delta_D}$) that on fly-by-wire aircraft are augmented by the Flight Control System (FCS) and subsequently sent to the aircraft controls through the servo-actuators ($\boldsymbol{\delta_S}$). The FCS often plays an important role in pilot-in-the-loop phenomena. It is worth noting that many of the problems discussed in [5] arise because of deficiencies in the FCS design where the possibility of indirect pilot activity from other axes contributing to instability in the control law's primary axis has not been considered in an appropriate manner. Thus, the FCS should be also included in the PVS. Unfortunately, FCS models are often available only in the later phases of design. However, it must be stressed that a robust FCS design to avoid PAO proneness, initiated during early design stages, will help to prevent these phenomena during flight tests.

The combined effect of the involuntary pilot action and control inceptor dynamics could be modeled through the biodynamic feed-through (BDFT), i.e. the transfer function between the accelerations measured at the pilot's seat, i.e. $\mathbf{y_A}$, and the control device deflections (pilot's demand) $\boldsymbol{\delta_D}$ obtained as output, see [13],

$$\boldsymbol{\delta_D} = \mathbf{H_{BDFT}}\left(s\right)\mathbf{y_A}. \tag{1}$$

Several pilot BDFT have been proposed in the literature using data from cockpit mock-up excitation, e.g.

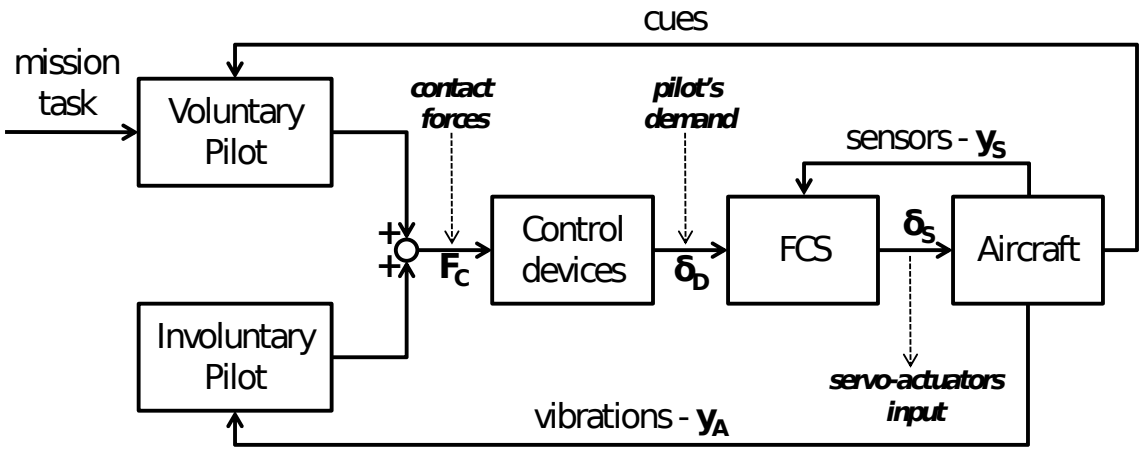

Figure 1. Flow block diagram of the PVS.

Allen et al. [14], Jex and Magdaleno [15] and Höhne [16], flight simulator tests, e.g. Mayo [17] and Masarati et al. [12], and in-flight measurements, e.g. Parham et al. [2]. Zanoni et al. [18] developed a detailed nonlinear multibody model for the characterization of the upper limbs of human operators, and used it to extract the BDFT.

BDFT has shown a large inter-subject, i.e. between different subjects, and intra-subject, i.e. on the same subject in different tests, variability. In fact, it is known that humans can adapt the dynamics of their limbs by adjusting their neuromuscular activation, depending on factors such as task goals, spatial position and orientation of the limbs, etc. (see Refs. [19, 20]), and it is likely that these adaptations have a significant influence on the resulting BDFT. Furthermore, it must be considered that the measured BDFT includes the control device dynamics. The contact forces generated by the pilot on the inceptor must react to the inertia, viscous and elastic restoring forces of the inceptor to reach the required deflection.

To separate the effects of the inceptor dynamics and modify the inceptor parameters in the BDFT, see Ref. [21], it is necessary to estimate the pilot's neuromuscular admittance (NMA), which is the dynamic relation between the pilot's control force $\mathbf{F_C}$ and the obtained deflection $\boldsymbol{\delta}_\mathbf{D}$, transforming the pilot biomechanics of equation (1) into

$$\boldsymbol{\delta}_\mathbf{D} = \mathbf{H}_\mathbf{BDFT}(s) \cdot \mathbf{y_A} + \mathbf{H}_\mathbf{NMA}(s) \cdot \mathbf{F_C}. \tag{2}$$

A method to identify the NMA from a detailed multibody model of the left upper limb has been proposed by Zanlucchi et al. in [21] and for both upper limbs by Zanoni et al. in [22]. Similarly, a technique to measure the

NMA via experimental tests from motion base simulators has been proposed by Venrooij et al. in [20]. The linearity of NMA and BDFT for small amplitude oscillations is verified both numerically and experimentally (see Refs. [14, 16, 17, 18, 19, 20, 21, 22]).

In tiltrotors the FCS can be separated into a primary flight control system (PFCS) and an automatic flight control system (AFCS) (see Ref. [2]). The PFCS contains the control laws necessary to maintain mission effectiveness, which include the pilot device gearing functions and rotor governor. The PFCS provides the necessary control mixing as a function of airspeed and conversion angle to permit a smooth transition between helicopter and airplane mode flight regimes and controls. The AFCS is designed to enhance flying qualities of the aircraft using feedback paths such as the pitch and roll rates. Consequently, in its simplest form the FCS could be described as

$$\boldsymbol{\delta}_{\mathbf{S}} = \mathbf{H}_{\mathbf{PFCS}}(s) \cdot \boldsymbol{\delta}_{\mathbf{D}} + \mathbf{H}_{\mathbf{AFCS}}(s) \cdot \mathbf{y}_{\mathbf{S}}, \tag{3}$$

where $(\mathbf{y}_{\mathbf{S}})$ are the aircraft sensors and $\boldsymbol{\delta}_{\mathbf{S}}$ is the servo input.

The aircraft model for PAO stability analyses can be also represented as a linearized system about a trim condition, described by the transfer matrix between the servo-actuator input $\boldsymbol{\delta}_{\mathbf{S}}$ and the output vector $\mathbf{y} = \{\mathbf{y}_{\mathbf{S}}, \mathbf{y}_{\mathbf{A}}, \dots\}$ containing the measures to close the feedback loop with the pilot and the FCS, namely:

$$\mathbf{y} = \mathbf{H}_{\mathbf{A/C}}(s, \mathbf{p}) \cdot \boldsymbol{\delta}_{\mathbf{S}}, \tag{4}$$

where the vector $\mathbf{p}$ contains the trim parameters.

In this work, only category I Rotocraft Pilot Couplings are analyzed [4], i.e. phenomena who do not imply a significant effect of nonlinearities (e.g. actuator saturations, freeplays, etc...). It can not be excluded that for large amplitude oscillations the nonlinearities may have an impact, although this is outside the scope of the research presented here.

In the following, Eqs. (1)-(4) will be defined for the Bell XV-15 tiltrotor, at the hover, sea-level standard (SLS) flight condition. The vertical bounce phenomenon will be investigated considering only the main vertical dynamics and the PVS will be reduced to a Single Input Single Output (SISO) system considering only the direct path between the power lever deflection as pilot's demand, $\boldsymbol{\delta}_{\mathbf{D}} = \delta_{PL}$, and the vertical acceleration measured at the pilot's seat, namely $\mathbf{y}_{\mathbf{A}} = a_z^{seat}$.

A. Aeroelastic tiltrotor model

To analyze the vertical bounce phenomenon in tiltrotors it is sufficient to consider the aircraft heave motion and the low-frequency out-of-plane wing bending dynamics. Due to the tiltrotor symmetry only half of the structure needs to be analyzed, as sketched in Fig. 2. The semi-span wing has been modeled as an elastic beam of length l and constant out-of-plane bending stiffness EI_{xx}, constrained to the plane of symmetry through a slider. The model is based on the XV-15 geometry, weights and wing structural characteristics reported in Ref. [11]. Two concentrated masses, located on the root (M_1) and on the tip of the wing (M_2), represent the fuselage-empennage and the nacelle-rotor bodies. The mass per unit-of-length of the semi-span wing has been lumped on its edges, so also included in M_1 and M_2, in order to obtain a simple analytical solution of the elastic problem. This approximation is considered acceptable to capture the low-frequency wing bending dynamics, since the wing mass is lower than the fuselage-empennage, nacelle and rotor masses placed on the wing edges. The percentage of lumped wing mass has been selected in order to improve the correlation with the modal mass and the mode shape of the first SWB mode of the XV-15 tiltrotor reported in Ref. [11]. Finally, a lumped inertia about the global x axis has been placed on the tip of the wing, i.e. $J_{xx}(\beta_n)$.

The kinematic of the wing is described as a function of the vertical displacement at the wing root $z(t)$ and of the vertical elastic deflection of the wing $w(y,t)$. The total vertical displacement is due to the sum of the two contributions. The elastic wing is modeled with the Euler-Bernoulli beam theory and the tiltrotor structural model can be obtained by the Principle of Virtual Work (PVW), namely:

$$\delta W = -\delta z M_1 \ddot{z} - (\delta z + \delta w_l) M_2 (\ddot{z} + \ddot{w}_l) - \delta w_l' J_{xx} \ddot{w}_l{}' - \int_0^l \delta w'' EI_{xx} w'' \mathrm{d}y = 0, \tag{5}$$

where the term $w_l = w(l,t)$ is introduced, i.e. the elastic deflection evaluated at the wing tip, the symbol δ is used to denote virtual quantities and $\mathrm{d}y$ represents the infinitesimal wing-span length. The analytical solution for the wing's deflection is:

$$w(y,t) = w_1(t)\frac{y^3}{6} + w_2(t)\frac{y^2}{2}, \tag{6}$$

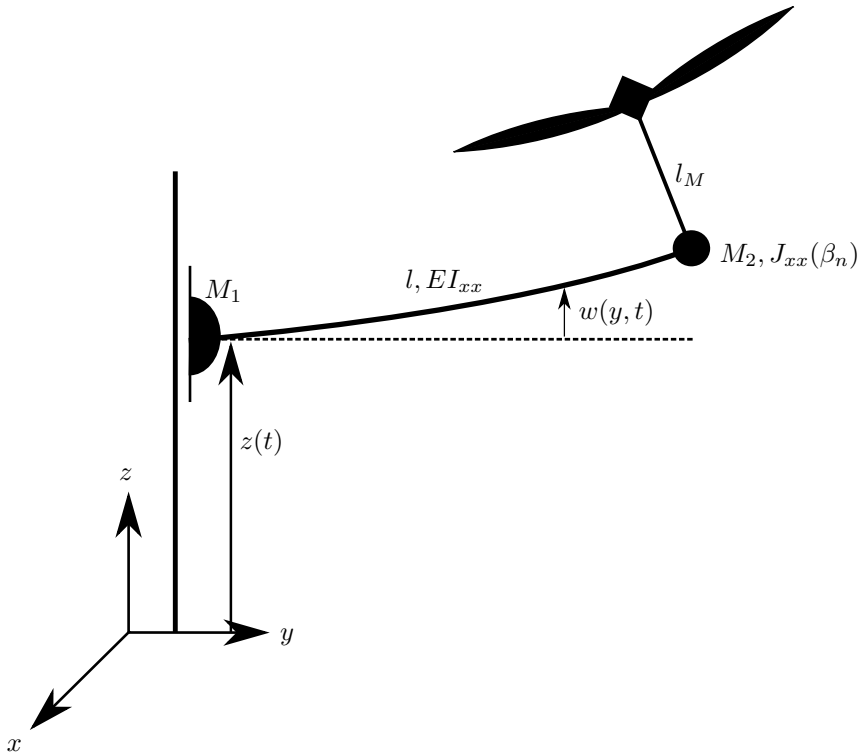

Figure 2. Sketch of the simplified tiltrotor model.

and the following second order model

$$\begin{bmatrix} M_1 + M_2 & M_2\frac{l^3}{6} & M_2\frac{l^2}{2} \\ M_2\frac{l^3}{6} & M_2\frac{l^6}{36} + J_{xx}\frac{l^4}{4} & M_2\frac{l^5}{12} + J_{xx}\frac{l^3}{2} \\ M_2\frac{l^2}{2} & M_2\frac{l^5}{12} + J_{xx}\frac{l^3}{2} & M_2\frac{l^4}{4} + J_{xx}l^2 \end{bmatrix} \begin{Bmatrix} \ddot{z} \\ \ddot{w}_1 \\ \ddot{w}_2 \end{Bmatrix} + EI_{xx} \begin{bmatrix} 0 & 0 & 0 \\ 0 & \frac{l^3}{3} & \frac{l^2}{2} \\ 0 & \frac{l^2}{2} & l \end{bmatrix} \begin{Bmatrix} z \\ w_1 \\ w_2 \end{Bmatrix} = \mathbf{0}, \tag{7}$$

describing the tiltrotor vertical dynamics in a vacuum. The model of Eq. (7) is used to evaluate frequencies and mode shapes in a vacuum for different tiltrotor configurations, updating the nacelle-rotor inertia J_{xx} as a function of the nacelle angle β_n.

The aerodynamic database is provided only in hover conditions including the rotor stability and control derivatives due to the rotor thrust force and the axial inflow dynamics described by Pitt-Peters in [23]. A simple perturbation model of the download acting on the wing is also included. The steady aerodynamic model must be able to capture the heave time constant and the first SWB aerodynamic damping. Rotor dynamics are not taken into account because their contribution is considered faster then the analyzed airframe

dynamics, thus negligible for modeling the vertical bounce phenomenon.

A steady, linearized, contribution of the thrust force produced by the rotor for the tiltrotor vertical dynamics includes the stability derivatives with respect to the vertical velocity measured at the rotor hub $\dot{z}_H$ and the axial (uniform) inflow λ_u, plus the control derivative due to the collective pitch ϑ_0:

$$\Delta T = -T_{/_{\dot{z}_H}} \dot{z}_H - T_{/_{\lambda_u}} \lambda_u + T_{/_{\vartheta_0}} \vartheta_0, \tag{8}$$

where the vertical velocity measured at the rotor hub is considered equal to the vertical velocity of the wing tip, i.e. $\dot{z}_H = \dot{z} + \dot{w}_l$. The virtual work due to the thrust perturbation, i.e. $\delta W = (\delta z + \delta w_l)\, \Delta T$, returns a damping matrix

$$\mathbf{C}_1 = T_{/_{\dot{z}_H}} \begin{bmatrix} 1 & \frac{l^3}{6} & \frac{l^2}{2} \\ \frac{l^3}{6} & \frac{l^6}{36} & \frac{l^5}{12} \\ \frac{l^2}{2} & \frac{l^5}{12} & \frac{l^4}{4} \end{bmatrix}, \tag{9}$$

and two input vectors

$$\mathbf{f}_1 = -T_{/_{\lambda_u}} \begin{bmatrix} 1 \\ \frac{l^3}{6} \\ \frac{l^2}{2} \end{bmatrix} \lambda_u + T_{/_{\vartheta_0}} \begin{bmatrix} 1 \\ \frac{l^3}{6} \\ \frac{l^2}{2} \end{bmatrix} \vartheta_0, \tag{10}$$

to be added to the second order model of Eq. (7). The thrust coefficients reported in Eq. (8) are obtained in this work through the blade element theory.

The download force acting on the wing is modeled as a vertical drag force distributed on the external sections of the tiltrotor wing as shown in Fig. 3. The dynamic pressure is due to the rotor wake induced velocity impacting downstream on the wing added to the wing vertical velocity, i.e. $v_w + (\dot{z} + \dot{w})$. During hover the rotor wake impinges on the wing with a velocity v_w that is related to the rotor disk induced velocity v through the conservation of mass. If A is the rotor disk area and A_w is the rotor wake area at the wing level,

$$v_w = v \left(\frac{A}{A_w} \right) = v \left(\frac{R}{R_w} \right)^2, \tag{11}$$

where it is possible to define a contraction factor $k = A/A_w = R^2/R_w^2$. The download in a hover condition can be evaluated through the strip theory integrating the download force per unit of length along the external

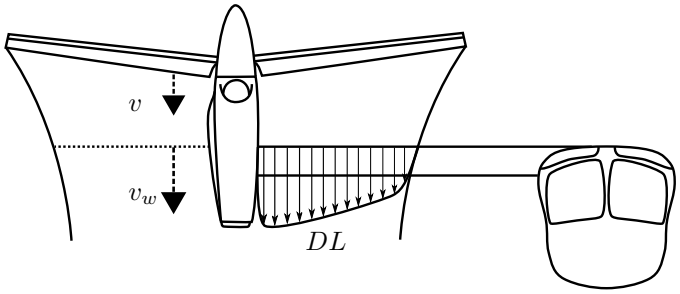

(a) Frontal view.

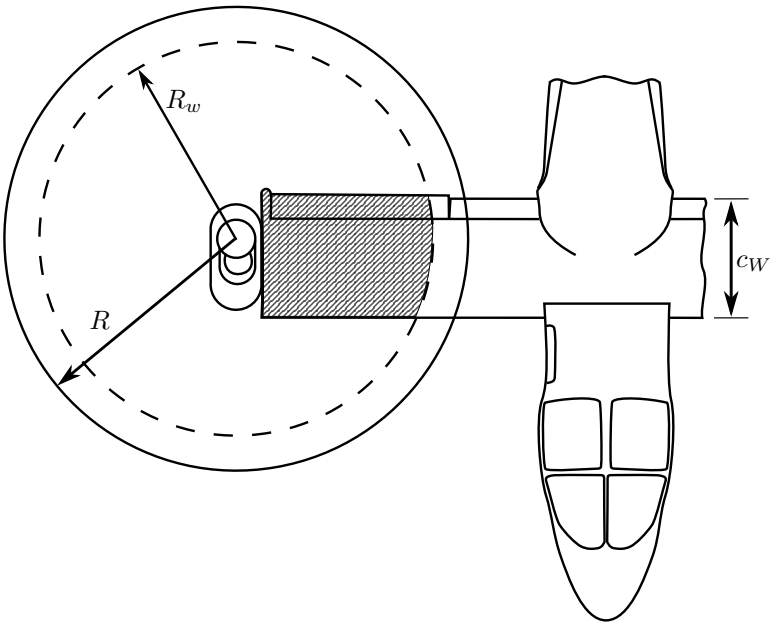

(b) Top view.

Figure 3. Tiltrotor wing subjected to download.

wing span:

$$DL_H = \int_{l-R_w}^{l} \frac{1}{2}\rho v_w^2 c_W\left(y\right) C_{DL} \mathrm{d}y, \tag{12}$$

where $c_W\left(y\right)$ is the tiltrotor wing chord, here considered constant. The aerodynamic download coefficient, C_{DL}, is roughly estimated as the drag coefficient of a 2D flat plate perpendicular to flow ($C_{DL} \approx 2$, see chapter 1 of ref. [24]), since the rotor wake is approximately orthogonal to the wing surface, obtaining:

$$\begin{aligned} DL_H &\approx \frac{1}{2}\rho v_w^2 c_W R_w C_{DL}, \\ &\approx \frac{1}{2}\rho k^2 v c_W \frac{R}{\sqrt{k}} C_{DL}, \\ &\approx \frac{1}{2}\rho k^{3/2} v c_W R C_{DL}. \end{aligned} \tag{13}$$

In a hover condition the download ranges from 10% to 15% of the overall tiltrotor weight, hence from the knowledge of DL_H it is possible to reverse Eq. (13) to obtain the contraction factor k. When considering the total velocity the download becomes:

$$DL = \int_{l-R_w}^{l} \frac{1}{2}\rho \left(v_w + \dot{z} + \dot{w}\right)^2 c_W\left(y\right) C_{DL} \mathrm{d}y, \tag{14}$$

and the linearized contribution about the hover trim condition on the PVW returns:

$$\delta W = -\int_{l-R_w}^{l} \left(\delta z + \delta w\right) \rho k v \left(k\Omega R \lambda_u + \dot{z} + \dot{w}\right) c_W\left(y\right) C_{DL} \mathrm{d}y, \tag{15}$$

where the rotor induced velocity perturbation has been introduced as function of the dimensionless inflow ratio $\lambda_u = \Delta v / \left(\Omega R\right)$. Defining the download coefficient per unit length, $DL_{/v} = \rho k v c_W C_{DL}$ which contains the constant term of Eq. (15), the PVW leads to an additional damping matrix

$$\mathbf{C}_2 = DL_{/v} \begin{bmatrix} R_w & \frac{1}{24}\left(l^4 - \left(l - R_w\right)^4\right) & \frac{1}{6}\left(l^3 - \left(l - R_w\right)^3\right) \\ \frac{1}{24}\left(l^4 - \left(l - R_w\right)^4\right) & \frac{1}{252}\left(l^7 - \left(l - R_w\right)^7\right) & \frac{1}{20}\left(l^5 - \left(l - R_w\right)^5\right) \\ \frac{1}{6}\left(l^3 - \left(l - R_w\right)^3\right) & \frac{1}{20}\left(l^5 - \left(l - R_w\right)^5\right) & \frac{1}{72}\left(l^6 - \left(l - R_w\right)^6\right) \end{bmatrix}, \tag{16}$$

and an input vector as a function of the dimensionless inflow:

$$\mathbf{f}_2 = -DL_{/v} k\Omega R \begin{bmatrix} R_w \\ \frac{1}{24}\left(l^4 - \left(l - R_w\right)^4\right) \\ \frac{1}{6}\left(l^3 - \left(l - R_w\right)^3\right) \end{bmatrix} \lambda_u. \tag{17}$$

The steady aerodynamic contributions due to the thrust and download perturbation are added to the mass and stiffness matrices of Eq. (7). After defining the state vector $\mathbf{u} = \{z, w_1, w_2\}^T$ and its time derivatives, the second order model takes the form:

$$\mathbf{M}\ddot{\mathbf{u}} + (\mathbf{C_1} + \mathbf{C_2})\,\dot{\mathbf{u}} + \mathbf{K}\mathbf{u} = \mathbf{f_1} + \mathbf{f_2}. \tag{18}$$

The proposed aeroelastic model is characterized only by the collective pitch as input. Servo-actuators are not included at this preliminary stage since the servo-valve dynamics have higher bandwidth compared to the vertical bounce phenomenon. The aircraft input can be directly considered as $\boldsymbol{\delta_S} = \vartheta_0$. Similarly, only the vertical acceleration at the pilot's seat, formally equal to the acceleration measured at the wing root $\mathbf{y_A} = a_z^{seat} = \ddot{z}$, is considered as output, returning a SISO model. The aircraft transfer matrix of Eq. (4) becomes a simple transfer function:

$$\ddot{z} = H_{\ddot{z}\vartheta_0}\,(s, \mathbf{p_H})\,\vartheta_0, \tag{19}$$

with the trim parameter vector evaluated at the hover condition $\mathbf{p_H}$.

The FCS is extremely simplified. In HEMODE, the PFCS includes only the gear ratio G_0 between the power lever displacement and the collective pitch rotation. The rotor governor has been neglected, under the hypothesis of constant rotor speed. Time delays can be introduced when considering FBW architectures, as for the V-22 or for the AW609. On the XV-15 tiltrotor, the pilot's controls were instantly transmitted to the servo-actuators through mechanical linkages [25]. Control laws on the vertical dynamics are usually not necessary, since they are asymptotically stable and easily controlled by the pilot. Hence, the AFCS is not included and the PFCS is represented by a simple gear ratio, i.e. $\vartheta_0 = G_0\delta_{PL}$. It must be noted that the gear ratio is scheduled with the nacelle angle. The highest value is obtained in HEMODE; then it decreases during the conversion, reaching zero in APMODE. Additionally, during hovering flight, the wing does not generate any aerodynamic contribution to increase the damping of the SWB mode. All these considerations make the hover condition one of the most critical for tiltrotor vertical bounce.

B. Validation results

The proposed aeroelastic (AE) tiltrotor model for vertical bounce analysis is based on the Bell XV-15, since the required data are available from the open literature. The structural characteristics are taken from the XV-15 finite element stick model of Ref. [11] and here reported in Table 1.

Table 1. XV-15 Structural model characteristics.

XV-15 Characteristic	Symbol	Value	Units
Fuselage mass[a]	M_F	6182.00	lb
Wing mass[b]	M_W	2534.00	lb
Left and right rotor masses	M_R	1118.00	lb
Left and right nacelle masses	M_N	3166.00	lb
Gross weight, $M_T = M_F + M_W + M_R + M_N$	M_T	13000.00	lb
Nacelle inertia about local[c] $\hat{x}$ axis	$J_{N_{\hat{x}\hat{x}}}$	100.00	slug-ft^2
Nacelle inertia about local[c] $\hat{z}$ axis	$J_{N_{\hat{z}\hat{z}}}$	450.00	slug-ft^2
Nacelle product of inertia about local[c] $\hat{x}\hat{z}$ axes	$J_{N_{\hat{x}\hat{z}}}$	0.00	slug-ft^2
Rotor mast length	l_M	4.67	ft
Wing semi-span length	l	16.08	ft
Wing beam stiffness	EI_{xx}	3.70E+09	lb-in^2

[a] Includes empennages, equipment, crew and payload.

[b] Includes fuel, cross shafting, etc.

[c] Aligned with the global reference frame in APMODE, rotating wrt. β_n.

The two lumped masses on the wing edges and the inertia on the wing tip have been evaluated considering the tiltrotor symmetry about the xz plane, namely:

$$M_1 = \frac{1}{2}\left(M_F + k_w M_W\right), \tag{20a}$$

$$M_2 = \frac{1}{2}\left(M_R + M_N + \left(1 - k_w\right) M_W\right), \tag{20b}$$

$$J_{xx}\left(\beta_n\right) = J_{N_{\hat{x}\hat{x}}} cos^2\beta_n + J_{N_{\hat{z}\hat{z}}} sin^2\beta_n - J_{N_{\hat{x}\hat{z}}} sin2\beta_n + \frac{1}{2} M_R \left(l_M sin\beta_n\right)^2, \tag{20c}$$

where k_w represents the percentage of wing mass lumped on the wing edges ranging from 0 to 1, and initially set to $k_w = 0.5$, to equally space the wing mass on the two edges. The inertia on the wing tip includes the nacelle contribution, reported in the global reference frame[b], and the inertia due to the rotor mass transport contribution. Considering these values as initial guess, the eigenanalysis of the simplified AE model in vacuum returns the SWB frequency and mode shape data reported in Table 2. The numerical values of k_w and EI_{xx} have been subsequently modified in order to reach the frequency and modal mass of the first SWB mode of the detailed XV-15 Finite Element Model (FEM) reported in Table 3 of Ref. [11], considering the APMODE configuration, i.e. $\beta_n = 0$ deg. Results are reported in Table 2.

Table 2. First SWB – Eigenanalysis results.

	FEM Model[a]	Proposed Model Initial Data	Proposed Model Updated Data
Percentage of wing mass lumped k_w, n.d.	-	0.5	0.8
Wing beam stiffness EI_{xx}, lb-in^2	-	3.70E+09	4.40E+09
Frequency, Hz	3.4	3.1	3.4
Modal mass, slug	241.6	306.4	241.6
Displacement at the wing tip, ft/ft	1.0000	1.0000	1.0000
Rotation at the wing tip, rad/ft	0.1463	0.1637	0.1486

[a] Table 3, Ref. [11].

The thrust stability and control derivatives in hover, SLS condition, have been roughly estimated with the

[b]The local nacelle reference frame is aligned with the global reference frame in APMODE. It can rotate with the nacelle angle β_n about the wing-span axis.

blade element theory considering blade constant contributions (see for example chapter 2 of [26]), namely:

$$T_{/\dot{z}_H} = \frac{B_T^2}{4R^2}\gamma N_b \Omega I_b, \tag{21a}$$

$$T_{/\lambda_u} = \frac{B_T^2}{4R}\gamma N_b \Omega^2 I_b, \tag{21b}$$

$$T_{/\vartheta_0} = \frac{B_T^3}{6R}\gamma N_b \Omega^2 I_b. \tag{21c}$$

Due to the tiltrotor symmetry, the thrust coefficient has been calculated considering half of the gross weight reported in Table 1,

$$C_{T_H} = \frac{M_T g/2}{\rho \left(\Omega R\right)^2 A^2}, \tag{22}$$

and the induced velocity with the actuator disk theory, namely

$$\frac{v}{\Omega R} = \kappa_h \sqrt{\frac{C_{T_H}}{2}}, \tag{23}$$

where an empirical inflow correction factor of $\kappa_h = 1.2$ has been taken into account. The XV-15 aerodynamic characteristics in Eqs. (21), (22) and (23) have been extracted from Ref. [27] (see Appendix B) and here reported in Table 3.

Table 3. XV-15 Aerodynamic model characteristics.

XV-15 Characteristic	Symbol	Value	Units
Number of blades per rotor	N_b	3	n.d.
Rotor radius	R	12.50	ft
Flapping inertia per blade	I_b	102.50	slug-ft^2
Rotor speed (HEMODE)	Ω	589.00	rpm
Lock number	γ	3.83	n.d.
Tip loss factor	B_T	0.97	n.d.
Empirical inflow correction factor in hover	κ_h	1.20	n.d.
Wing chord	c_W	5.25	ft

The time constant of the rigid heave dynamics has been compared with the results obtained by the Generic Tiltrotor simulation (GTRs) code in [28] and with the results identified during an experimental test

campaign of the XV-15 by Tischler with CIFER (Comprehensive Identification from FrEquency Responses), a system identification tool based on a comprehensive frequency-response approach [29]. The eigenvalues are listed in Table 4. Frequency and damping of the first SWB mode are also reported for the AE model, including the structural damping of 3% as described by Acree et al. in [11]. Results obtained with the

Table 4. Aeroelastic roots

	GTRs	CIFER	AE Model W/out download	AE Model With download
Heave-mode time constant, sec	4.99	9.52	5.01	4.32
First SWB Frequency, Hz	-	-	3.18	3.18
First SWB Damping[a], %	-	-	3.86	3.90

[a] Includes a 3% of structural damping [11].

GTRs and CIFER represent only the rigid, low frequency, behavior of the XV-15. The comparison of the heave-mode time constant shows a good correlation with the GTRs data but a poor correlation with the flight-extracted results identified by CIFER. Both the GTRs code and the AE model underestimate the heave-mode time constant. Tiltrotor class vehicles, in contrast to single-rotor helicopters, are characterized by very long time-constants due to the higher disk loading [29] and probably the representation of the aerodynamic loads on the GTRs code and on the AE model is not sufficiently accurate to correctly capture the heave dynamics. Although the simplified AE model is artificially modified to obtain the same heave-mode time constant — this could be easily obtained by reducing the stability derivative of the thrust as a function of the vertical speed — the vertical bounce phenomenon would still persist, since it is located in a higher frequency range, close to 3 Hz.

The aerodynamic forces slightly increase the damping of the first SWB. A small contribution of less than 1% is added to the prescribed structural damping (3%). The aerodynamic damping in hover is mainly produced by the rotors and the wing does not generate any aerodynamic contribution. The low damping of the first SWB mode in hover and its proximity to the pilot's biomechanical pole make the vehicle more prone to the instability. Including the wing download, the first SWB damping weakly increases (+ 0.04%) while the heave-mode time constant is reduced from 5.01 to 4.32 sec.

The transfer function (TF) of the vertical acceleration response $\ddot{z}$ to the power-lever δ_{PL} is reported in Fig. 4(a). The bode plot shows the TF of the proposed AE model with those obtained with the GTRs and CIFER. The comparison is made in a frequency range up to 1 Hz since the GTRs and CIFER do not represent the higher aeroelastic frequency content. Again, there is a good correlation between the results of the AE model and the GTRs code, proving that both models are able to develop the same control forces. Conversely, the magnitude of the TF identified by CIFER is lower, showing that all numerical models seem to overestimate the control forces produced by the rotors. A higher value of the vertical acceleration due to power-lever input is considered conservative for the analysis of the vertical bounce phenomenon, especially during the initial vehicle design. The effect of the higher vertical acceleration predicted by the numerical model is also shown in Fig. 4(b), where the time response to the power-lever input is obtained directly from flight test data and compared with the results obtained by the model identified by CIFER and with the proposed AE model. The AE model is able to capture only the overall trend recorded during the flight test, providing higher values of the vertical acceleration at the same power-lever input. Finally, it should be noted that the flight test data also show a higher frequency contribution probably related to the first SWB between 21–25 seconds.

C. Validation with a higher order numerical model

To verify the simple aeroelastic tiltrotor model presented in this work, a detailed aeroservoelastic model of the XV-15 was realized using data from [27, 11, 30]. The model was built using the simulation tool MASST (Modern Aeroservoelastic State Space Tools), developed at Politecnico di Milano for the aeroservoelastic and aeromechanical analysis of aircraft and rotorcraft [31, 32].

The dynamic model set-up includes: 1) the airframe structural stick model [11], 2) airframe unsteady aerodynamics, 3) rotor aeroelastic models, 4) a lumped parameter engine drive-train model, 5) servo-actuators dynamics and 6) a rotor speed governor controller. Rotor aeroelastic models were obtained in CAMRAD/JA using data published by Acree in Ref. [30]. Collective and cylic modes were considered for the three bladed stiff-in-plane gimballed rotor of the XV-15. In particular, three bending and two torsion modes were represented plus the two rigid gimbal modes. The rotor speed degree of freedom was also accounted to connect the rotors to the drive train torsional model. Rotor aerodynamics was based on blade element and momentum

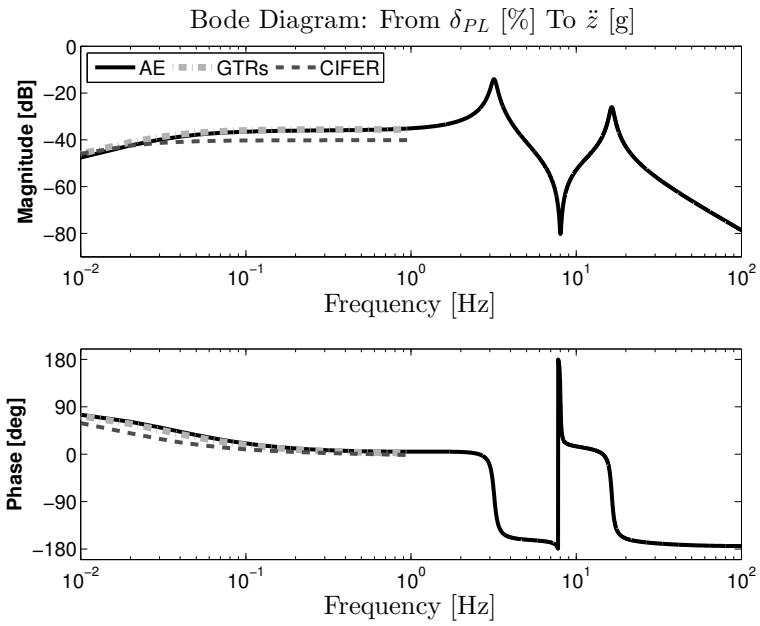

(a) Transfer Function (see Fig. 4.27, pag. 85, of Ref. [29]).

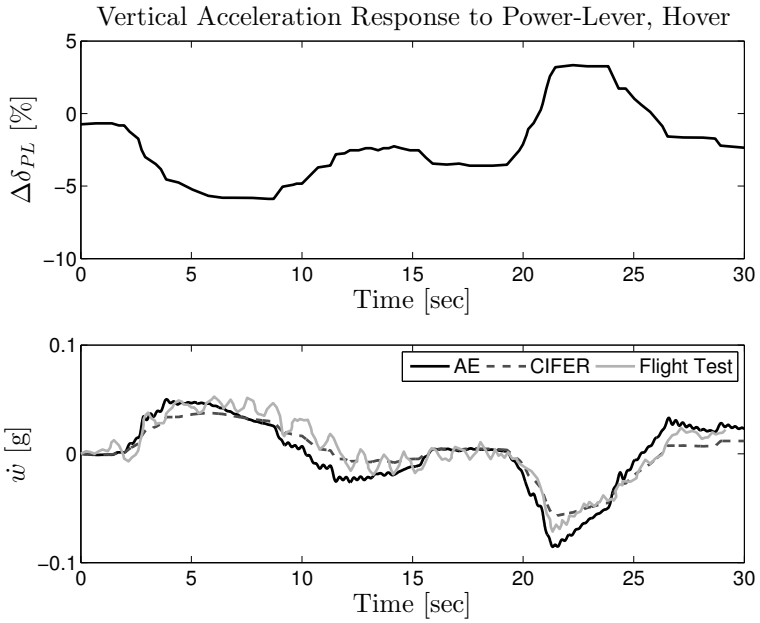

(b) Time Response (see Fig. 4.34, pag. 97, of Ref. [29]).

Figure 4. Vertical acceleration response to power-lever input.

theory, using Pitt–Peters' dynamic inflow model. A lumped torsional drive train system was created following the physical architecture of a symmetric transmission. Engines and rotors were simplified as lumped inertias, such as all the components related to the transmission gearings. The model was condensed in order to obtain a simplified torsional model to be used for the complete dynamic system compatibility. Data were

obtained from Ref. [30]. Servo-actuators were represented by transfer functions that model the servo-valve and compliance dynamics (see chapter 6 of Ref. [33]). Finally, a rotor speed governor was introduced as a feedback controller to maintain constant RPM. A collective pitch governing scheme ("Beta" governor) is generally used for tiltrotors [34]. In helicopter mode there is a direct function between PL and collective pitch which is scheduled with nacelle angle, i.e. $G_0(\beta_n)$. In airplane mode this value becomes null. This input is summed with the rotor speed governor output, namely ϑ_{gov}, to establish blade pitch. A feedforward line is also present between the PL and the engine power, through the throttle control, i.e. ϑ_t, also controlled by the PL input through the gear ratio G_t. The "Beta" governor block scheme is shown in Fig. 5.

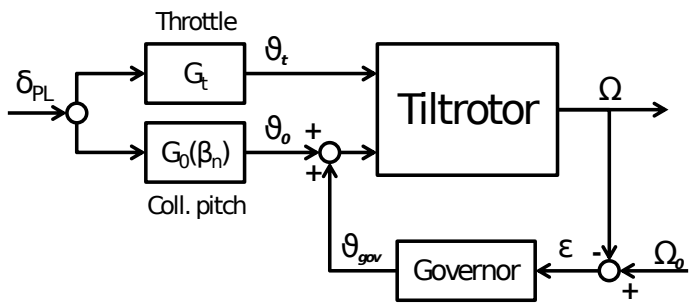

Figure 5. "Beta" governor block scheme.

The rotor speed governor is a proportional plus integral (PI) controller which establishes a collective pitch command through the feedback of the error between commanded and measured RPM. The governor dynamics are represented by a second order lag [35]. Both the proportional and integral feedback gains are reported in tables 17-I and 17-II of Ref. [27], scheduled with the nacelle angle. In helicopter mode the proportional path minimized RPM excursions during higher frequency PL activity, while the integral path eliminated steady state error [34]. It must be noted that the MASST model is representative of the XV-15 Research Aircraft with Advanced Technology Blades (ATBs) [30]. Rotor characteristics, with composite blades, are slightly different from those reported in Table 3, which are for the original XV-15 tiltrotor with metallic blades. To compare the simplified AE model with the detailed MASST model it is necessary to modify the rotor parameters, according to Ref. [30].

Results are shown in terms of transfer functions between the power-lever deflection δ_{PL} and the vertical acceleration at the pilot's seat $\ddot{z}$. Figure 6 shows that the simplified AE model is able to capture the low-

frequency dynamics, including the SWB mode. The heave-mode time constants are equal to $\tau = 4.69$ sec for the MASST model and $\tau = 4.35$ sec for the simplified AE model. The SWB frequency is well captured although the damping ratio is slighly lower (smaller than 1%) on the AE model. The rotor collective dynamics are placed in the next decade. The first lead-lag mode is coupled with the symmetric drive-train mode at 12.8 Hz while the symmetric rotor coning mode is found at 15.7 Hz. Kinematic blade pitch/bending couplings, included in the MASST model, are not significant. The blade mode shapes are not rigid, since they involve the elastic deformation of the rotor yoke, although the equivalent (or virtual) lead-lag and flap hinges result quite close to the pitch horn–pitch link connection. The pitch/bending coupling coefficients are both positive (stable pitch/flap and pitch/lag couplings). Conversely, gimbal rotors are characterized by a negative pitch/gimbal (δ_{3G} = -15 deg.) such as the rotor of the XV-15. A negative δ_{3G} is necessary to obtain flap-lag stability in high-speed airplane mode, as discussed by Parham et al. in Ref. [3]. However, the pitch/bending and pitch/gimbal coupling effects do not show significant differences on the vertical dynamics between the simplified and the detailed model close to the SWB mode (see Fig. 6). Moreover, the firsts rotor collective modes are above 10 Hz, far away from the SWB mode, including the rotor coning. Lower frequency rotor dynamics could be related to the gimbal regressive modes. However, a collective pitch input due to the power-lever cannot excite the gimbal dynamics, that is composed by cyclic modes.

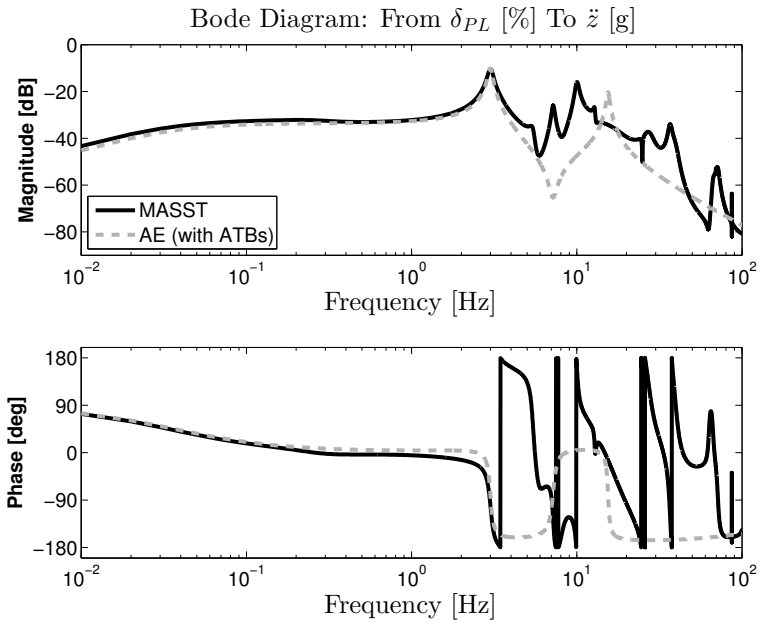

Figure 6. MASST vs AE (with ATBs): vertical acceleration response to power-lever input.

The rotor governor affects the power-lever to thrust response, so it was decided to analyze its impact on the tiltrotor vertical dynamics. Figure 7 compares two MASST models obtained with and without the governor. In this case a smaller heave-subidence time constant ($\tau = 3.89$ sec) is obtained, but the response in the frequency range of interest (i.e. up to 4 Hz) remains unchanged. These results show that, for a preliminary vertical bounce analysis in hover condition, the governor dynamics can be neglected. So, it is verified that the AE model is fully representative of the dynamics that influence the phenomenon under investigation.

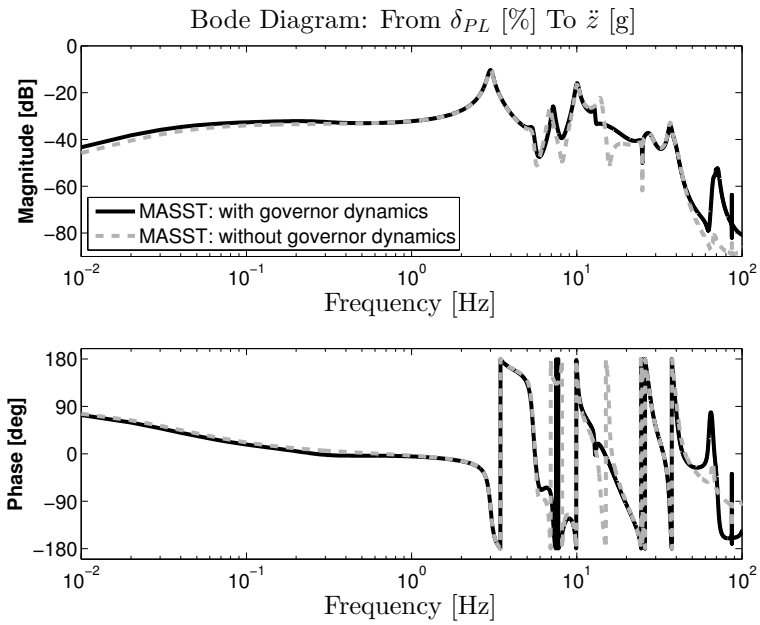

Figure 7. Governor effect on the vertical acceleration response to power-lever input.

D. Pilot-control device biomechanical models

Mayo [17] identified a simple model for BDFT of a human body to describe the involuntary action of helicopter pilots on the collective control inceptors when subjected to vertical vibration of the cockpit. In particular, Mayo identified the TFs between the absolute vertical acceleration of the pilot hand, $\ddot{z}_{h.abs}$, as a function of the vertical acceleration of the vehicle, $\ddot{z}$. Two sets of pilots have been considered, called ectomorphic (small and lean build) and mesomorphic (large bone structure and muscle build). As discussed in [9], these TFs need to be written as the relative acceleration of the hand, $\ddot{z}_{hand}$, with respect to the vehicle acceleration, and integrated two times to regain a low-frequency correct behavior, resulting in

$$H_{BDFT}(s) = -\frac{s}{(s+\omega_h)^2}\frac{s+1/\tau_p}{s^2+2\xi_p\omega_p s+\omega_p^2}, \tag{24}$$

where a numerical value of $\omega_h = 3.10$ rad/s has been used in Eq. (24). The maximum vertical displacement of the XV-15 power-lever inceptor, $z_{hand}^{MAX} = 10.0$ inches (see Ref. [27]), has been used to obtain a dimensionless output of Eq. (24).

The poles associated with the pilot's BDFT are well damped (about 30%). The frequency is about 3.5 Hz, compared with the "three cycles per second" mentioned in the vertical bounce accidents[c].

A pilot-control device model in the form of Eq. (2) can be obtained through a rational representation of both the BDFT and NMA transfer functions, consisting of a second-order low-pass filter in the band of interest (1-10 [Hz]) as suggested by Zanlucchi et al. in [21], namely:

$$H_{(\cdot)}(s) = \frac{b_{(\cdot)}}{s^2+a_1 s+a_2}, \tag{25}$$

with $(\cdot)$ corresponding to BDFT and NMA. Eq. (25) can be used to describe the basic pilot biomechanical behavior and also to analyze the effects of modifications to the dynamics of the control inceptor on the overall dynamics of the vehicle. In this work, the TFs coefficients have been tuned considering Mayo's models as a starting point. In particular:

- the denominator coefficients a_1, a_2 have been defined in order to obtain the same damping and characteristic frequency of the Mayo's model's biomechanical poles, i.e. $a_2 = \omega_p^2$ and $a_1 = 2\xi_p\omega_p$;
- the BDFT numerator b_{BDFT} has been defined in order to perfectly match the Mayo model's pilot

[c] NTSB reports SEA08LA043 and ANC08LA083, see the webpage: http://www.ntsb.gov

biomechanical magnitude at the characteristic frequency, i.e. $b_{BDFT} \rightarrow \|H_{BDFT}(\mathrm{j}\omega_p)\|$, where ω_p is the frequency of the biodynamic pole (see Fig. 8(a));

- the NMA numerator b_{NMA} has been calculated in order to obtain a force gradient, considering a static reference condition, of about 9 $lb_f/\%$.

The identified coefficients of the second-order pilot-control device BDFT and NMA TFs are reported in Table 5 considering ectomorphic and mesomorphic pilot's characteristics. It should also be noted that

Table 5. Structural properties of second-order pilot-control device model.

Ectomorphic Pilot	Symbol	Value	Units
Denominator	a_2	452.30	$(\mathrm{rad/sec})^2$
Denominator	a_1	13.70	rad/sec
Numerator BDFT	b_{BDFT}	-1.07	rad^2
Numerator NMA	b_{NMA}	-5.15	rad^2/slinch
Mesomorphic Pilot	**Symbol**	**Value**	**Units**
Denominator	a_2	555.40	$(\mathrm{rad/sec})^2$
Denominator	a_1	13.31	rad/sec
Numerator BDFT	b_{BDFT}	-1.07	rad^2
Numerator NMA	b_{NMA}	-6.90	rad^2/slinch

the proposed second-order pilot-control device model overlaps with the pilot's voluntary behavior. The introduction of a high-pass filter, with a cut-off frequency above the crossover frequency, can be used to solve this problem.

The knowledge of the NMA allows modification of the control device dynamics. For example, it is possible to include a hydraulic damper in the power-lever to decrease the vertical bounce proneness. Considering a linear damper, the pilot's force acting on the control device will be characterized by two contributions, namely:

$$F_C = C\dot{\delta}_{PL} + \hat{F}_C, \tag{26}$$

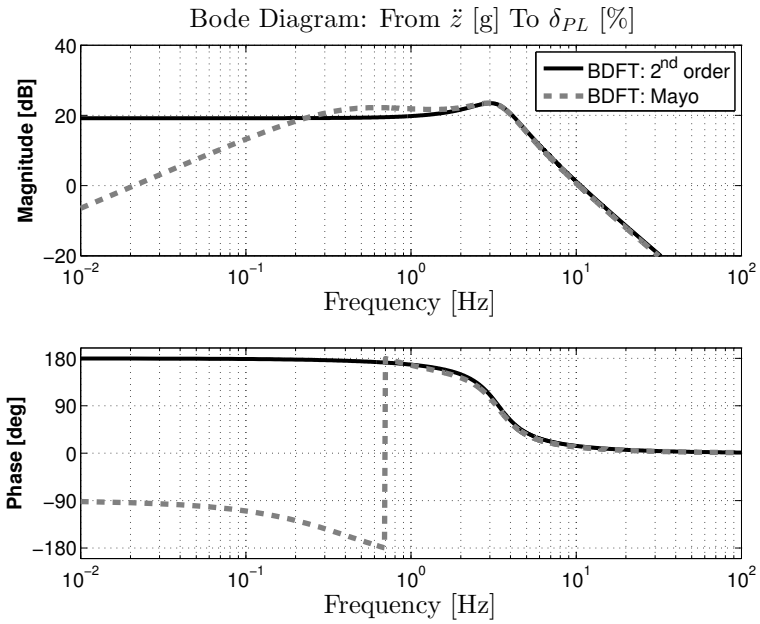

(a) Biodynamic Feedthrough (BDFT).

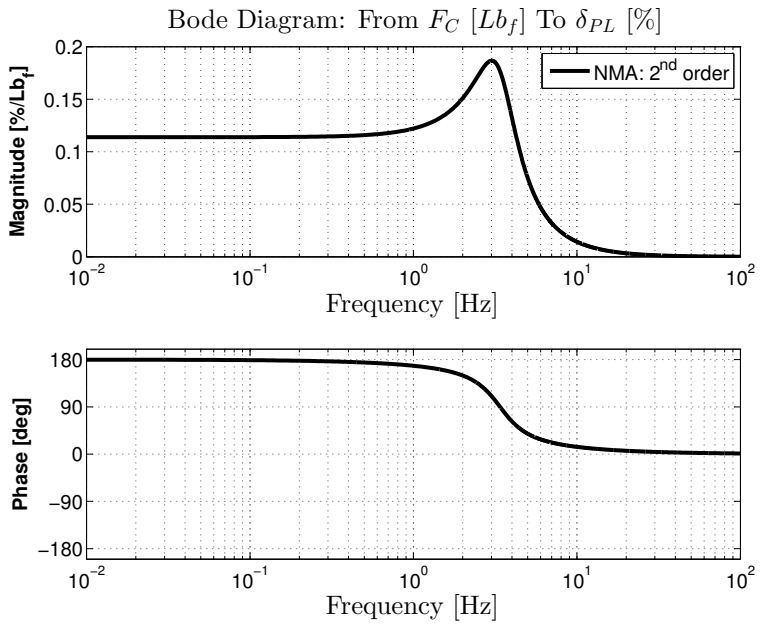

(b) Neuromuscular Admittance (NMA).

Figure 8. Pilot-control device second-order numerical model of Mayo's ectomorphic TF.

where the first term is the viscous force produced by the damper and the second contribution an additional force acting on the device. Applying Eq. (26) in the second-order pilot-control device model, the following transfer functions are obtained:

$$\delta_{PL} = \frac{b_{BDFT}}{s^2 + a_1 s + a_2}\ddot{z} + \frac{b_{NMA}}{s^2 + a_1 s + a_2}\left(Cs\delta_{PL} + \hat{F}_C\right), \tag{27}$$

which yields an updated pilot-control device BDFT and NMA TFs,

$$H'_{BDFT}(s) = \frac{b_{BDFT}}{s^2 + (a_1 - b_{NMA} \cdot C)\, s + a_2}, \tag{28a}$$

$$H'_{NMA}(s) = \frac{b_{NMA}}{s^2 + (a_1 - b_{NMA} \cdot C)\, s + a_2}, \tag{28b}$$

acting on the damping ratio of the biomechanical pole. It should be noted that the term b_{NMA} is negative, hence the introduction of the simple linear damper returns a higher damping ratio on the pilot-control device dynamics.

III. Loop closure on the vertical axis

The vertical axis loop is closed by feeding the pilot-control device BDFT to the tiltrotor AE model through the appropriate gear ratio between the collective pitch rotation and the power-lever vertical displacement, equal to $G_0 = \partial\vartheta_0/\partial\delta_{PL} = 1.6$ deg/in for the analyzed HEMODE configuration (see Table 8a-IV of Ref. [27]). The power lever input might also add a term δ'_{PL} (e.g. due to a voluntary pilot model[d]) to the pilot's BDFT, which yields

$$\delta_{PL} = H_{BDFT}(s)\,\ddot{z} + \delta'_{PL}, \tag{29}$$

fed into the tiltrotor TF of Eq. 19 through the collective pitch gear ratio,

$$\left(1 - G_0 H_{BDFT} H_{\ddot{z}\vartheta_0}\right)\ddot{z} = G_0 H_{\ddot{z}\vartheta_0}\delta'_{PL}. \tag{30}$$

The Loop Transfer Function (LTF) is thus the coefficient of $\ddot{z}$ in Eq. (30) minus 1, namely:

$$H_{LTF} = -G_0 H_{BDFT} H_{\ddot{z}\vartheta_0}. \tag{31}$$

With the proposed SISO analytical model it is possible to investigate the stability of the PVS and the sensitivity of the stability to several design parameters. Instead of using the classical eigenvalues investigation, in

[d]For example, a pilot model able to keep the altitude of the aircraft with an adequate voluntary collective control input. A model of voluntary behavior of the pilot is proposed by McRuer and Jex in Ref. [36].

this case it is possible to exploit the robust stability analysis approach, because it gives information about the grade of stability with respect to parameter variations [37, 38, 39]. The Nyquist criterion is very explicative because it intuitively expresses the stability degree of robustness as the distance of each point of the LTF frequency response from the point $(-1 + \mathrm{j}0)$ in the Argand diagram (see chapter 7 of Ref. [40]). Robust stability indices are phase (P_M) and gain (G_M) margins. The phase margin is the phase difference between the crossing of the LTF with the unit circle and -180 deg., namely $180 - \angle H_{LTF}\left(\mathrm{j}\omega_{|H_{LTF}|=1}\right)$. The gain margin is $1/H_{LTF}\left(\mathrm{j}\omega_{(-180)}\right)$, i.e. the inverse of the LTF magnitude at ω corresponding to -180 deg of phase. Positive margins indicate a stable system, while to obtain robust systems it is usually necessary to reach gain margins above 6 dB and phase margins of 60 deg.

A. Stability predictions

Results in the present section highlight the proneness of the XV-15 tiltrotor to vertical bounce according to the simplified AE model. Initially, Mayo's ectomorphic TF has been introduced in the LTF of Eq. (31). The robust analysis (see Fig. 9) returns an unstable condition characterized by negative gain and phase margins. The PVS shows that the direct effect of a change in collective input results in a nearly immediate change in thrust, which accelerates the tiltrotor exciting the lightly damped first SWB and, in turn, the pilot's biomechanics. The phenomenon appears as a resonance between the two modes, hence completely different from the vertical bounce mechanism triggered in helicopters, in which the highly damped first rotor collective flap mode (rotor coning) reduces the phase margin of the pitch-heave loop TF [9]. In tiltrotors, it is preferred that the gain margin is reduced when the pilot-control device BDFT closes the feedback loop with the low-frequency aircraft structural dynamics.

It should be remembered that the proposed AE tiltrotor model is conservative for vertical bounce analyses, since it is characterized by an overestimated control derivative T_{ϑ_0} and it neglects the stabilizing effect due to the power-lever friction. The PVS is also characterized by several uncertainties: the pilot-control device BDFT identified by Mayo was obtained on a flight simulator that differ from the XV-15 cockpit with dissimilar control-device dynamics, as well as the strong impact of the neuromuscular activity discussed at the beginning of this work.

Nevertheless, there are two key points making the tiltrotor prone to the vertical bounce phenomenon:

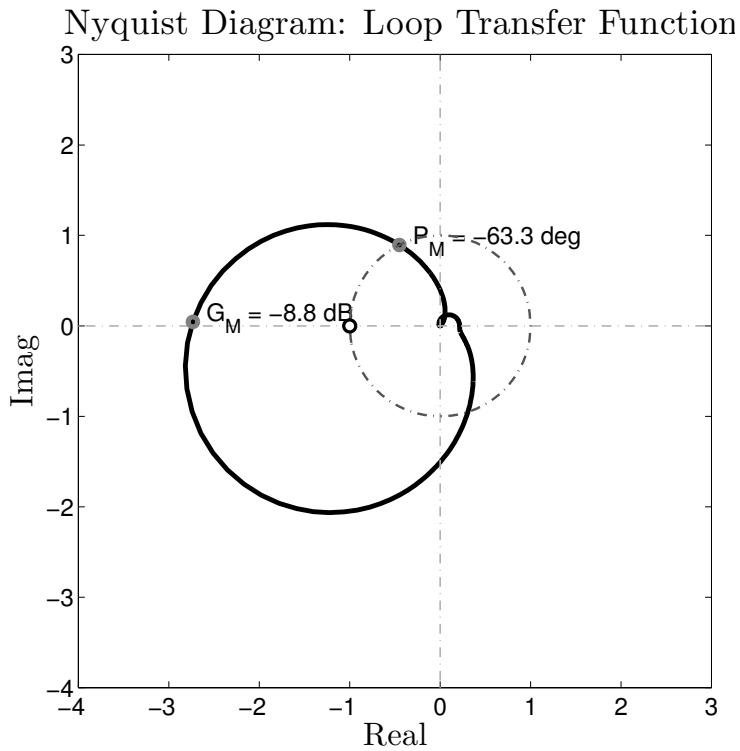

(a) Nyquist diagram.

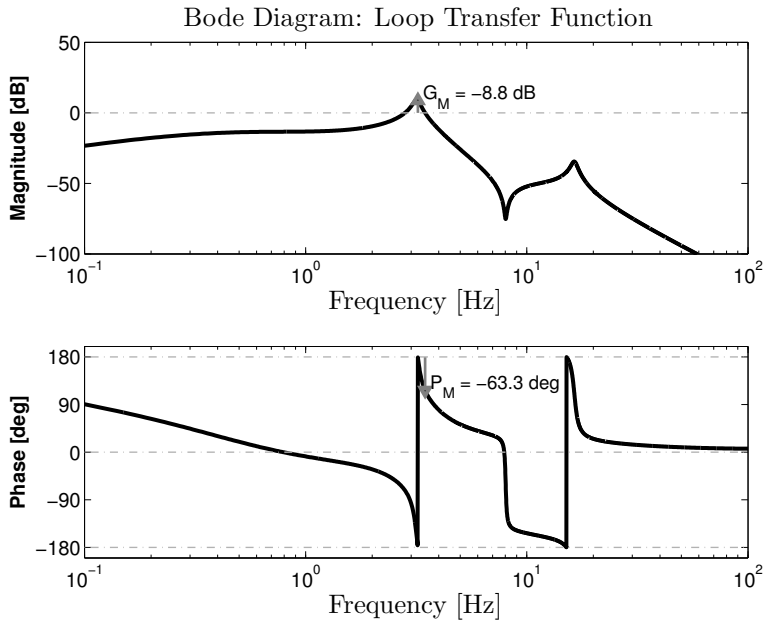

(b) Bode diagram.

Figure 9. LTF with Mayo's ectomorphic pilot-control device BDFT.

1. the closeness of the first SWB frequency to the pilot's biomechanical pole;

2. the light damping of the first SWB mode;

which might bring a PVS close to the resonance.

Sensitivity analyses in Fig. 10 show the bode diagrams of the LTF for several configurations with different gross weight, operating conditions, pilot-control device models and wing bending stiffness. The PVS are always characterized by negative stability margins. Figure 10(a) shows the LTF for different values of

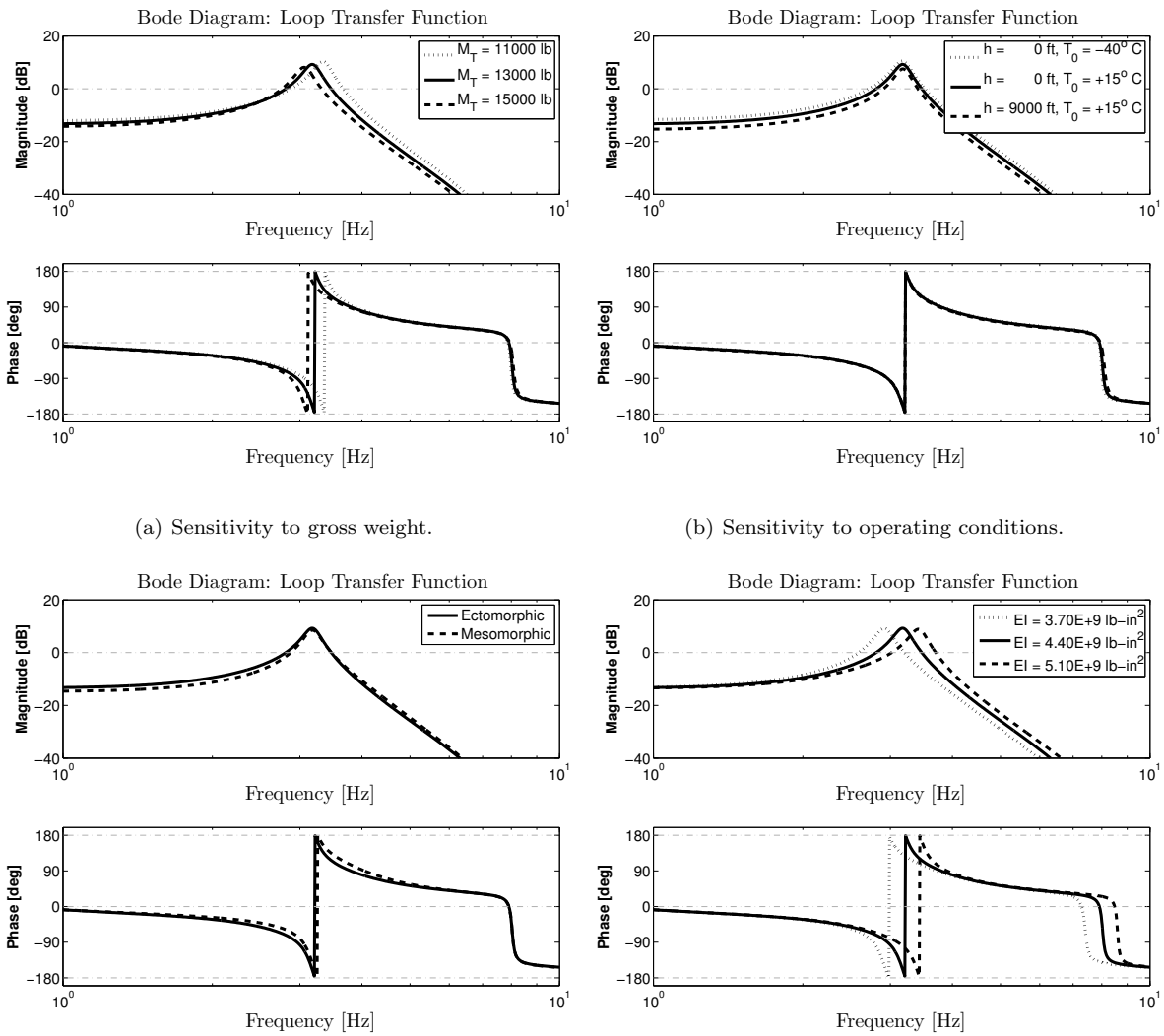

(a) Sensitivity to gross weight.

(b) Sensitivity to operating conditions.

(c) Sensitivity to pilot-control device models.

(d) Sensitivity to wing bending stiffness.

Figure 10. Sensitivity analyses to PVS parameters.

gross weight. Results are compared between the standard configuration at 13,000 lb and for the light/heavy weight configurations reported in the flight envelope (see Ref. [25]). A change in the gross weight modifies the

frequency of the first SWB mode and thus the gain and phase margins of the PVS. Results improve slightly when increasing the tiltrotor gross weight up to 15,000 lb. Increasing the weight, the first SWB frequency is reduced (from 3.18 to 3.06 Hz, hence a bit more distant from the ectomorphic pilot's biomechanical pole at 3.38 Hz) and the negative gain/phase margins are reduced. Opposite results are obtained when reducing the gross weight, since the lower weight first SWB frequency (3.35 Hz when M_T = 11,000 lb) is closer to the pilot's biomechanical pole. Figure 10(b) shows the LTF bode diagrams for different operating conditions. When operating at ISA -40° C the air density increases by about +23%; when operating at 9,000 ft the air density decreases by about -23%. The air density mainly acts on the control derivative $T_{\vartheta_0} \propto \rho \rightarrow \gamma$, increasing the stability margins at higher altitudes through a reduction of the pilot control effectiveness. Sensitivity analyses for the ectomorphic and mesomorphic pilot-control device BDFT models are shown in Fig. 10(c). Results are quite similar. Although the mesomorphic pilot's biomechanical pole is characterized by a smaller damping ratio (ξ_{Ecto} = 32% vs ξ_{Meso} = 28%), the ectomorphic pilot's frequency is closer to the first SWB mode, hence to the resonance condition. Finally, modification of the wing bending stiffness is considered. Figure 10(d) shows the different bode diagrams for three values of EI_{xx} ranging up ± 16% from the nominal value. None of these three configurations shows a stable situation. The first SWB frequency ranges from 2.93 Hz (EI_{xx} = 3.7E+9 lb-in^2) to 3.44 Hz (EI_{xx} = 5.1E+9 lb-in^2); still too close to the pilot-control device biomechanical pole. All numerical data obtained with the analyzed configurations are reported in Table 6. The worst case scenario results for case number 2, at SLS ISA condition, with Mayo's ectomorphic pilot and light weight configuration.

B. Means of prevention

The previous discussion highlighted how the vertical bounce in tiltrotors is due to the resonance between the pilot-control device biomechanical pole and the lightly damped first SWB mode. Prevention requires either reducing involuntary collective control, or reducing its effect on the vertical acceleration of the cockpit. Possible means are:

1. apply friction to the power-lever, which requires the pilot to overcome a threshold reaction force to actually move the device;

2. modify the combined pilot-control device BDFT acting on the control device dynamics; a possible

Table 6. XV-15 analyzed configurations.

Case no.	Pilot	Gross Weight M_T, lb	Altitude h, ft	Temperature T_0, ^{o}C	Wing Stiffness EI_{xx}, lb-in^2	SWB Freq. ω_{SWB}, Hz	SWB Damp. ξ_{SWB}, %	Gain Margin G_M, db	Phase Margin P_M, db
1	Ecto	13,000	0.0	15.0	4.40E+9	3.18	3.90	-8.8	-63.3
2	Ecto	11,000	0.0	15.0	4.40E+9	3.35	3.82	-10.2	-73.5
3	Ecto	15,000	0.0	15.0	4.40E+9	3.06	3.96	-7.4	-54.1
4	Ecto	13,000	0.0	-40.0	4.40E+9	3.18	4.11	-9.9	-67.1
5	Ecto	13,000	9000.0	15.0	4.40E+9	3.19	3.69	-7.1	-57.4
6	Meso	13,000	0.0	15.0	4.40E+9	3.18	3.90	-7.0	-45.5
7	Ecto	13,000	0.0	15.0	3.70E+9	2.93	3.96	-7.9	-50.8
8	Ecto	13,000	0.0	15.0	5.10E+9	3.44	3.86	-8.7	-71.9

solution is to add a hydraulic damper on the PL to further increase the damping of the biomechanical pole;

3. redesign the control-device; for example by replacing the power-lever with the thrust control lever used in the V-22 ;

4. filter the unwanted dynamics at the FCS level.

On point 3 it is useful to recall that for the V-22 case the change of inceptors layout with respect to the XV-15 led to other RPC biodynamic problems [2, 5]. Additionally, the implications of such a change in terms of ergonomy and ease of handling by pilots may go well beyond a simple fix on one of the aircraft systems, eventually leading to a complete redesign of the aircraft. Consequently, we decided to focus just on two means of prevention: the first is based on the design of a notch filter (active device); while the second is obtained by adding a hydraulic damper, with linear characteristics, to the power-lever (passive device), that can be partially representative also of the effect of friction. The design takes into account the XV-15 flight envelope for the analyzed hover configuration, considering a test matrix for all the combinations of #1 gross weight (11,000 lb $< M_T <$ 15,000 lb), #2 operative conditions (from SLS ISA-40°C to FL090) and #3 pilot-control device BDFT models (ectomorphic and mesomorphic). Once the worst case scenario is identified, the devices are designed to obtain a stable and robust PVS with a gain margin above 6 db and a phase margin of (at least) 60 degrees.

Notch Filters (NFs) are intended to suppress the resonance peaks of the undesired modes, expressed in terms of LTF (see Ref. [41]). They are characterized by second-order transfer functions of the form:

$$H_{NF}(s) = \frac{1 + c_1 s + c_2 s^2}{1 + c_3 s + c_4 s^2}, \tag{32}$$

where c_1, c_2, c_3 and c_4 are the NF coefficients. However, it may be useful to adopt a different set of parameters which are more directly related to the NF features. In particular, four parameters can be selected for each NF:

1. the notch frequency ω_{NF}, where the maximum decline in gain should be observable;
2. the slope in gain μ (in dB) at the notch frequency;
3. the quality factor Q, where the effects of NFs are significant;
4. the non dimensional gain value μ_∞ for infinite frequency.

NF coefficients and parameters are related to each other through the following expressions (see Ref. [41]):

$$\omega_{NF} = \frac{1}{\sqrt{c_2}}, \tag{33a}$$

$$\mu = 20log\left(\frac{c_1}{c_3}\right), \tag{33b}$$

$$Q = \frac{\sqrt{c_4}}{c_3}, \tag{33c}$$

$$\mu_\infty = \frac{c_2}{c_4}. \tag{33d}$$

In this way, such parameters can be easily selected when analyzing the characteristics of the signal component which should be filtered. The selected parameters have been optimized to make sure that the tiltrotor, equipped with the FCS, satisfies the robust stability criteria. Furthermore, the NF parameters should not be dependent on flight conditions and aircraft configurations in order to achieve a realistic clearance procedure. In this work, a single NF has been designed after an optimization process considering the test matrix defined at the beginning of this section. An envelope of all LTFs for the different flight conditions and configurations is estimated. Results are shown in Fig. 11(a). Starting from the bode diagrams of all the LTFs, the LTF envelope is built. The NF frequency and slope in gain have been selected in order to suppress the highest resonance peak below the threshold of -6 db (ω_{NF} = 3.35 Hz, μ = -25 db) to satisfy the gain margin

requirement. The quality factor has been selected to maintain the LTF envelope below the threshold of -6 db for all the frequency band close to the NF frequency ($Q = 0.833$). Finally, a unitary non dimensional gain value for infinite frequency has been chosen to restore the frequency content over the first SWB mode. The phase behavior is shown in Fig. 11(b). The designed NF also satisfies the phase margin requirement restoring a robust PVS. However, it should be noted that the introduction of NF in the aircraft FCS produces a phase loss in the LTFs (with NF included) that acts in the low-frequency domain, with negative effects on aircraft flight dynamics stability. Hence, to optimize the NF it is necessary to limit its effect only in the frequency range of interest . The designed NF introduces a phase delay of about -20 deg at 1 Hz and the phase loss is reduced for the lower frequencies. The phase loss may be not negligible when considering the additional phase related to the vehicle dynamics, including the FCS control laws, the servo dynamics, etc. The possibility to design scheduled notch filters for the different flight conditions could fix this problem, despite the complexity for the FCS.

The design of the hydraulic damper on the power-lever can be achieved with the modified pilot-control device BDFT of Eq. (28a) introduced in the LTF of Eq. (31). In this case, for each condition of the test matrix, the viscous coefficient has been evaluated in order to satisfy the robust stability conditions. Results are shown in Fig. 12. The critical condition has been obtained for the light weight configuration (M_T = 11,000 lb), SLS ISA-40°C operating conditions and with the ectomorphic pilot. The designed viscous coefficient is equal to C = 2500 lbf-in/(rad/sec), increasing the damping ratio of the ectomorphic pilot's biomechanical pole from the original $\xi_{Ecto} = 32\%$ to $\xi_{Ecto+C} = 51\%$. This solution is also able to return a stable (and robust) PVS, although it presents several drawbacks: the phase delay effect is not localized only about the resonance peak but also in the low-frequency flight dynamics bandwidth; moreover the hydraulic damper on the power-lever increases the pilot's reaction force to move the device and to control the vehicle.

With the designed hydraulic damper, a pilot's inceptor force F_c of about 20 lbf is necessary to rotate a power-lever with a length of 1 ft at a harmonic input of 1 Hz[e]; clearly an unrealistic force that no pilot would tolerate. The design of a hydraulic damper that stabilizes the PVS, with an acceptable reaction force increment, is still possible although it will not satisfy the robust conditions.

[e]A rough estimate of the reaction force due to the hydraulic damper is possible in the frequency domain since: $F_C = \mathrm{j}\omega C \delta_{PL}$.

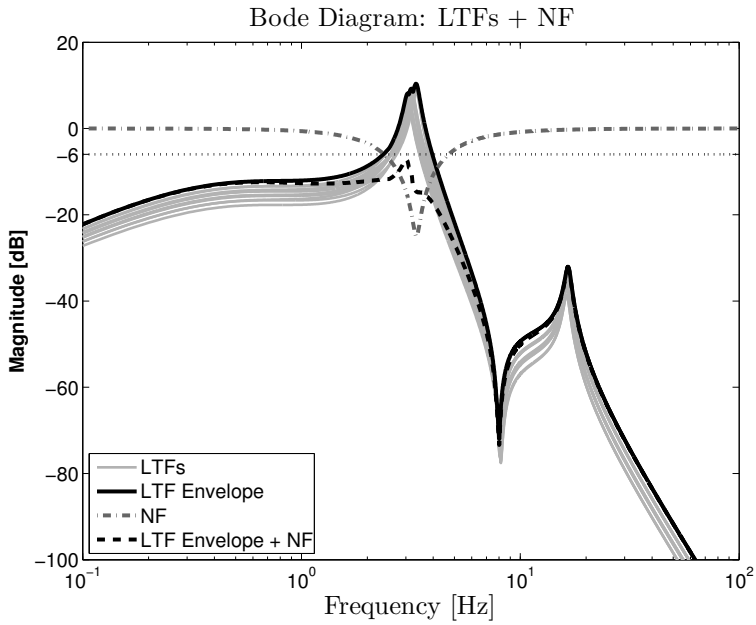

(a) Magnitude.

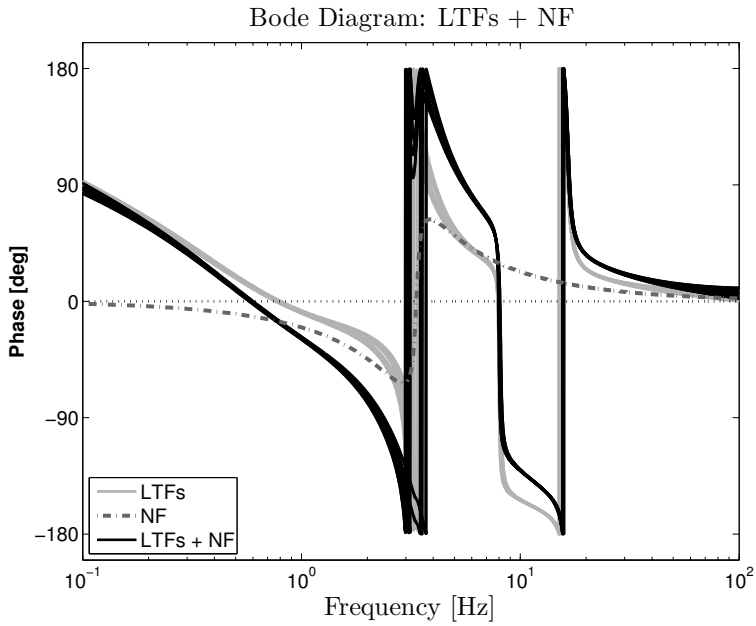

(b) Phase.

Figure 11. Robust design of the NF.

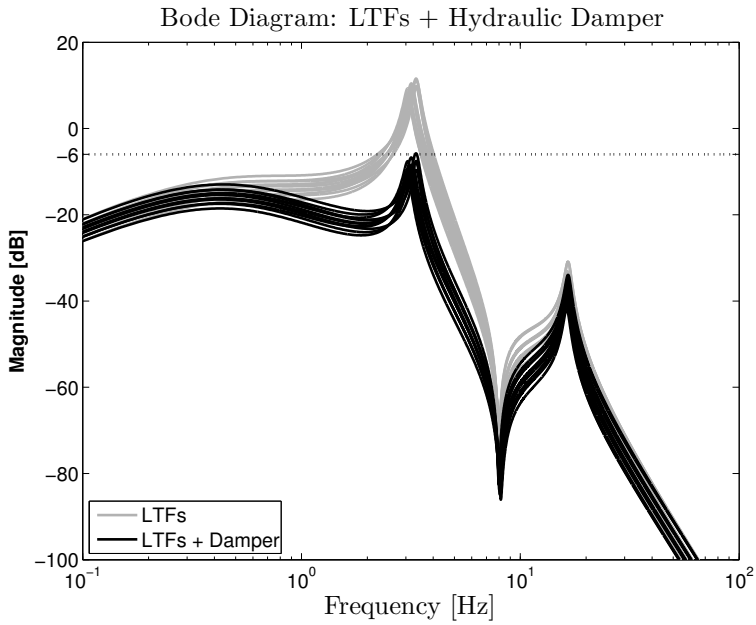

(a) Magnitude.

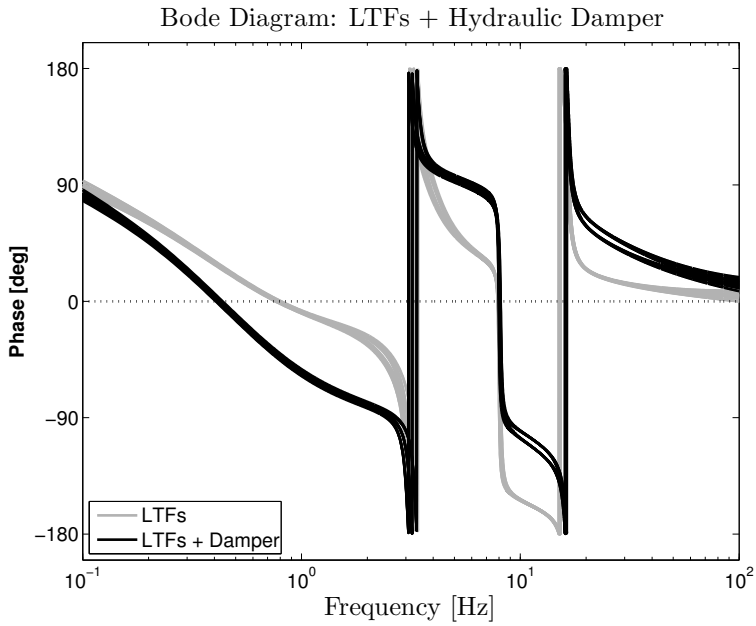

(b) Phase.

Figure 12. Robust design of the hydraulic damper.

In summary, the proposed means of prevention are both able to restore a robust system, although some drawbacks must be taken into account. The notch filter can be easily implemented in aircraft with FBW architectures. However, the frequency range of interest is very close to the FCS bandwidth, so a detailed analysis should consider the impact of the NF on the handling qualities and PIO tendency of the aircraft. The hydraulic damper can be directly installed on the power-lever as a simple mechanical device. In this case the pilot–control device damping is artificially increased, although the reaction force exerted by the pilot to control the power lever can easily grow up to a level where the easiness of handling could be compromised. Consequently, a thorough evaluation of the impact of these modifications on the flight mechanics of the aircraft is necessary.

IV. Conclusions

This work describes the vertical bounce phenomenon in tiltrotors for the case of hovering flight, a Pilot-Assisted Oscillation (PAO) instability that may arise as a resonance between the pilot's biomechanical pole and the aircraft's poorly damped first Symmetric Wing Bending (SWB) mode. It differs from the mechanism triggered in helicopters, in which the highly damped first rotor collective flap mode (rotor coning) reduces the phase margin of the pitch-heave loop transfer function.

It has been found that there are two key factors making the tiltrotor prone to the vertical bounce phenomenon: first the closeness of the first SWB frequency with the pilot's biomechanical pole, and second the light damping of the first SWB mode (reduced in hover because the wing is not producing any aerodynamic force). The vertical bounce phenomenon can be triggered when a vertical power-lever is installed in the cockpit, since it increases the transmissibility between the vertical acceleration at the pilot's seat and the unintentional vertical response of the pilot's upper limb due to biodynamics. Sensitivity analyses for different gross weight, operating conditions, pilot-control device Biodynamic Feedthrough (BDFT) models and wing bending stiffness show that it is not easy to determine the design parameters to avoid the vertical bounce, although several means of prevention are available. Two examples are reported: a structural notch filter on the collective control path and a hydraulic damper on the power-lever. Both are able to stabilize the vehicle with robust stability margins though some drawbacks are present. The notch filter is usually optimized for one particular flight condition or aircraft configuration. Scheduled notch filters, as a function of the flight

conditions and aircraft configurations, must be consequently taken into account, increasing the complexity of the flight control system (FCS). Another solution is to design a hydraulic damper that acts mainly on the damping ratio of the pilot-control device BDFT, restoring a stable pilot-vehicle system. To satisfy the robust stability margins, however, huge viscous coefficients are necessary, increasing drastically the pilot's reaction force to move the device and to control the vehicle. The availability of a simple yet representative low-order model for this PAO phenomenon may be of great help in the design of the aircraft FCS. In fact, knowing from the early stage of development that there are marginally stable feedback loops between the aircraft structure and the pilots biodynamics may lead to a more robust design of the FCS, with the possibility of including these elements as additional constraints during its design.

References

[1] Bilger, J., Marr, R., and Zahedi, A., "Results of Structural Dynamic Testing of the XV-15 Tilt Rotor Research Aircraft," *Journal of the American Helicopter Society*, Vol. 27, No. 2, 1982, pp. 58–65, doi:10.4050/JAHS.27.58.

[2] Parham, Jr., T., Popelka, D., Miller, D. G., and Froebel, A. T., "V-22 Pilot-in-the-Loop Aeroelastic Stability Analysis," *American Helicopter Society 47th Annual Forum*, Phoenix, Arizona (USA), May 6–8 1991.

[3] Parham, Jr., T. and Corso, L. M., "Aeroelastic and Aeroservoelastic Stability of the BA 609," *25th European Rotorcraft Forum*, Rome, Italy, September 14–16 1999, pp. G3–1–10.

[4] Dieterich, O., Götz, J., DangVu, B., Haverdings, H., Masarati, P., Pavel, M. D., Jump, M., and Gennaretti, M., "Adverse Rotorcraft-Pilot Coupling: Recent Research Activities in Europe," *34th European Rotorcraft Forum*, Liverpool, UK, September 16–19 2008.

[5] Walden, R. B., "A Retrospective Survey of Pilot-Structural Coupling Instabilities in Naval Rotorcraft," *American Helicopter Society 63rd Annual Forum*, Virginia Beach, VA, May 1–3 2007, pp. 1783–1800.

[6] Pavel, M. D., Masarati, P., Gennaretti, M., Jump, M., Zaichik, L., Dang-Vu, B., Lu, L., Yilmaz, D., Quaranta, G., Ionita, A., and Serafini, J., "Practices to Identify and Preclude Adverse Aircraft-and-

Rotorcraft-Pilot Couplings — A Design Perspective," *Progress in Aerospace Sciences*, Vol. 76, 2015, pp. 55–89, doi:10.1016/j.paerosci.2015.05.002.

[7] Gennaretti, M., Serafini, J., Masarati, P., and Quaranta, G., "Effects of Biodynamic Feedthrough in Rotorcraft-Pilot Coupling: Collective Bounce Case," *Journal of Guidance, Control, and Dynamics*, Vol. 36, No. 6, 2013, pp. 1709–1721, doi:10.2514/1.61355.

[8] Masarati, P., Quaranta, G., Lu, L., and Jump, M., "A Closed Loop Experiment of Collective Bounce Aeroelastic Rotorcraft-Pilot Coupling," *Journal of Sound and Vibration*, Vol. 333, No. 1, January 2014, pp. 307–325, doi:10.1016/j.jsv.2013.09.020.

[9] Muscarello, V., Quaranta, G., and Masarati, P., "The Role of Rotor Coning in Helicopter Proneness to Collective Bounce," *Aerospace Science and Technology*, Vol. 36, July 2014, pp. 103–113, doi:10.1016/j.ast.2014.04.006.

[10] Acree, Jr, C. W. and Tischler, M. B., "Identification of XV-15 Aeroelastic Modes Using Frequency-Domain Methods," TM 101021, NASA, 1989.

[11] Acree, Jr, C. W., Peyran, R. J., and Johnson, W., "Rotor Design for Whirl Flutter: An Examination of Options for Improving Tiltrotor Aeroelastic Stability Margins," *American Helicopter Society 55th Annual Forum*, Montréal, Quebec, Canada, May 25–27 1999.

[12] Masarati, P., Quaranta, G., and Jump, M., "Experimental and Numerical Helicopter Pilot Characterization for Aeroelastic Rotorcraft-Pilot Couplings Analysis," *Proc. IMechE, Part G: Journal of Aerospace Engineering*, Vol. 227, No. 1, January 2013, pp. 124–140, doi:10.1177/0954410011427662.

[13] Quaranta, G., Masarati, P., and Venrooij, J., "Impact of Pilots' Biodynamic Feedthrough on Rotorcraft by Robust Stability," *Journal of Sound and Vibration*, Vol. 332, No. 20, September 2013, pp. 4948–4962, doi:10.1016/j.jsv.2013.04.020.

[14] Allen, R. W., Jex, H. R., and Magdaleno, R. E., "Manual Control Performance and Dynamic Response During Sinusoidal Vibration," TR 73-78, AMRL, October 1973.

[15] Jex, H. R. and Magdaleno, R. E., "Biomechanical Models for Vibration Feedthrough to Hands and Head for a Semisupine Pilot," *Aviation, Space, and Environmental Medicine*, Vol. 49, No. 1–2, 1978, pp. 304–316.

[16] Höhne, G., "Computer Aided Development of Biomechanical Pilot Models," *Aerospace Science and Technology*, Vol. 4, No. 1, January 2000, pp. 57–69, doi:10.1016/S1270-9638(00)00117-6.

[17] Mayo, J. R., "The Involuntary Participation of a Human Pilot in a Helicopter Collective Control Loop," *15th European Rotorcraft Forum*, Amsterdam, The Netherlands, 12–15 September 1989, pp. 81.1–12.

[18] Zanoni, A., Masarati, P., and Quaranta, G., "Rotorcraft Pilot Impedance from Biomechanical Model Based on Inverse Dynamics," *International Mechanical Engineering Congress & Exposition (IMECE) 2012*, Houston, Texas, November 9–15 2012, Paper No. IMECE2012-87533.

[19] Venrooij, J., Abbink, D. A., Mulder, M., van Paassen, M. M., and Mulder, M., "Biodynamic Feedthrough is Task Dependent," *2010 IEEE International Conference on Systems Man and Cybernetics (SMC)*, Istanbul, Turkey, October 10–13 2010, pp. 2571–2578, doi:10.1109/ICSMC.2010.5641915.

[20] Venrooij, J., Abbink, D. A., Mulder, M., van Paassen, M. M., and Mulder, M., "A Method to Measure the Relationship Between Biodynamic Feedthrough and Neuromuscular Admittance," *IEEE Transactions on Systems, Man, and Cybernetics, Part B: Cybernetics*, Vol. 41, No. 4, 2011, pp. 1158–1169, doi:10.1109/TSMCB.2011.2112347.

[21] Zanlucchi, S., Masarati, P., and Quaranta, G., "A Pilot-Control Device Model for Helicopter Sensitivity to Collective Bounce," *ASME IDETC/CIE 2014*, Buffalo, NY, August 17–20 2014, DETC2014-34479.

[22] Masarati, P., Quaranta, G., and Zanoni, A., "A Detailed Biomechanical Pilot Model for Multi-Axis Involuntary Rotorcraft-Pilot Couplings," *41st European Rotorcraft Forum*, Munich, Germany, September 1–4 2015.

[23] Pitt, D. M. and Peters, D. A., "Theoretical Prediction of Dynamic-Inflow Derivatives," *Vertica*, Vol. 5, No. 1, 1981, pp. 21–34.

[24] Anderson, Jr., J. D., "Fundamentals of Aerodynamics," chap. 1, McGraw-Hill, New York, 2010.

[25] Maisel, M., "NASA/Army XV-15 Tilt-Rotor Research Aircraft Familiarization Document," TM X-62,407, NASA, January 1975.

[26] Johnson, W., "Helicopter Theory," chap. 2, Princeton University Press, Princeton, New Jersey, 1980.

[27] Ferguson, S. W., "A Mathematical Model for Real Time Flight Simulation of a Generic Tilt-Rotor Aircraft," CR 166536, NASA, 1988.

[28] Ferguson, S. W., "Development and Validation of a Simulation for a Generic Tilt-Rotor Aircraft," CR 166537, NASA, 1989.

[29] Tischler, M. B., "Frequency-Response Identification of the XV-15 Tilt-Rotor Aircraft Dynamics," TM 89428, NASA, 1987.

[30] Acree, Jr, C. W., "An Improved CAMRAD Model for Aeroelastic Stability Analysis of the XV-15 With Advanced Technology Blades," TM 4448, NASA, 1993.

[31] Masarati, P., Muscarello, V., and Quaranta, G., "Linearized Aeroservoelastic Analysis of Rotary-Wing Aircraft," *36th European Rotorcraft Forum*, Paris, France, September 7–9 2010, pp. 099.1–10.

[32] Masarati, P., Muscarello, V., Quaranta, G., Locatelli, A., Mangone, D., Riviello, L., and Viganò, L., "An Integrated Environment for Helicopter Aeroservoelastic Analysis: the Ground Resonance Case," *37th European Rotorcraft Forum*, Gallarate, Italy, September 13–15 2011, pp. 177.1–12.

[33] Merritt, H. E., "Hydraulic Control Systems," chap. 6, John Wiley & Sons, New York, 1967.

[34] Schaeffer, J., Alwang, R., and Joglekar, M., "V-22 Thrust Power Management Control Law Development," *American Helicopter Society 47th Annual Forum*, Phoenix, Arizona (USA), May 6–8 1991.

[35] Johnson, W., *CAMRAD/JA, A Comprehensive Analytical Model of Rotorcraft Aerodynamics and Dynamics, Johnson Aeronautics Version*, Johnson Aeronautics, 1988.

[36] McRuer, D. T. and Jex, H. R., "A Review of Quasi-Linear Pilot Models," *Human Factors in Electronics, IEEE Transactions on*, Vol. HFE-8, No. 3, September 1967, pp. 231–249, doi:10.1109/THFE.1967.234304.

[37] Quaranta, G., Muscarello, V., and Masarati, P., "Lead-Lag Damper Robustness Analysis for Helicopter Ground Resonance," *Journal of Guidance, Control, and Dynamics*, Vol. 36, No. 4, July 2013, pp. 1150–1161, doi:10.2514/1.57188.

[38] Quaranta, G., Tamer, A., Muscarello, V., Masarati, P., Gennaretti, M., Serafini, J., and Colella, M. M., "Rotorcraft Aeroelastic Stability Using Robust Analysis," *CEAS Aeronautical Journal*, Vol. 5, No. 1, March 2014, pp. 29–39, doi:10.1007/s13272-013-0082-z.

[39] Muscarello, V., Masarati, P., and Quaranta, G., "Robust Stability Analysis of Adverse Aeroelastic Roll/Lateral Rotorcraft-Pilot Couplings," *Journal of the American Helicopter Society*, Vol. 62, No. 2, 2017, pp. 1–13.

[40] Skogestad, S. and Postlethwaite, I., "Multivariable Feedback Control," chap. 7, John Wiley & Sons, Chichester, 2005.

[41] Battipede, M., Gili, P., Carano, L., and Vaccaro, V., "Constrained Notch Filter Optimization for a Fly-By-Wire Flight Control System," *l'Aerotecnica Missili e Spazio*, Vol. 88, No. 3, 2009, pp. 105–113.